Journal of Ethnopharmacology 371 (2026) 122117

Contents lists available at ScienceDirect

Journal of Ethnopharmacology

journal homepage: www.elsevier.com/locate/jethpharm

Metabolite profiling and in vitro assessment of skin-related pharmacological activities in *Baccharis trimera* (Less.) DC

Philipp Gabor [a,1], Wéldion G. Mesquita Júnior [b,1], Kyuri Ribeiro [b], Romário Pereira da Costa [b], Quezia B. Cass [c], Vanessa Gisele Pasqualotto Severino [d], Richele P. Severino [b], Geísa Ferreira Costa Makishi [e], Gislane Florambel Siqueira [e], Matthias F. Melzig [a], Alexander Weng [a,*], Lorena R.F. de Sousa [b,**]

[a] *Institute of Pharmacy, Freie Universität Berlin, Berlin, 14195, Germany*
[b] *Institute of Chemistry, Federal University of Catalão, Catalão, Goiás, 75704-020, Brazil*
[c] *Chemistry Department, Federal University of São Carlos, São Carlos, São Paulo, 13565-905, Brazil*
[d] *Chemistry Institute, Federal University of Goiás, Goiânia, Goiás, 74690-900, Brazil*
[e] *Livealoe, Itapuranga, Goiás, 76680-000, Brazil*

ARTICLE INFO

Keywords:
Anti-inflammatory
Elastase
Tyrosinase
THP-1
Cosmeceutical

ABSTRACT

Ethnopharmacological relevance: Baccharis trimera (Less.) DC. (Asteraceae), commonly known as "carqueja", is a medicinal plant traditionally used in Brazil as an herbal remedy for gastrointestinal disorders. In some regions, its aerial parts are also used to treat skin-related diseases, including wounds. Despite growing interest in discovering new cosmeceutical ingredients from traditionally used medicinal plants, knowledge of this species and its potential skin-related applications remains limited.

Aim of the study: We investigated the aerial parts of *B. trimera* for their anti-inflammatory, anti-aging, and skin-whitening properties.

Materials and methods: The ethanolic extract (*Bt*E) was fractionated via liquid-liquid extraction into hexane (*Bt*EH), dichloromethane (*Bt*ED), ethyl acetate (*Bt*EA), and hydroalcoholic (*Bt*EHy) fractions. Chemical dereplication of *Bt*E and active fractions (*Bt*EA and *Bt*ED) was performed using liquid chromatography coupled with high-resolution mass spectrometry (LC–HRMS). Enzyme inhibitory activity against tyrosinase and elastase was evaluated spectrophotometrically. Anti-inflammatory activity was assessed in lipopolysaccharide (LPS)-stimulated THP-1 macrophages by quantifying TNF-α, IL-1β, and IL-6 levels using ELISA.

Results: The crude extract inhibited elastase activity, while its fractions reduced cytokine production and enhanced tyrosinase inhibition. Among these, the dichloromethane fraction showed the most pronounced effects, including tyrosinase inhibition, reduced secretion of TNF-α, IL-1β and IL-6, and a significant decrease in LPS-induced LDH release. Twenty compounds, including flavonoids, hydroxycinnamic acid derivatives, diterpenes, phenylpropanoids, and fatty acids, were annotated in the active ethanolic extract and its fractions from *Baccharis trimera*, several of which have previously shown anti-inflammatory activity. After fractionation, cirsimaritin, eupatorin, and jaceosidin were found exclusively in the dichloromethane fraction and may have contributed to its anti-inflammatory activity. In addition, the anti-tyrosinase activity observed in the medium-polarity fractions may be associated with the presence of rutin, apigenin flavone glucoside, and 3-hydroxy-copalic acid.

Conclusion: Overall, this study expands the chemical characterization of this medicinal plant and underscores its potential for skincare applications. Notably, anti-tyrosinase activity was identified in the medium-polar fractions for the first time, highlighting their potential as a source of bioactive metabolites relevant for cosmetic and skin-related applications.

* Corresponding author.
** Corresponding author.
E-mail addresses: alexander.weng@fu-berlin.de (A. Weng), lorennarf@ufcat.edu.br (L.R.F. Sousa).
[1] These authors contributed equally to this work.

https://doi.org/10.1016/j.jep.2026.122117
Received 5 April 2026; Received in revised form 21 June 2026; Accepted 25 June 2026
Available online 25 June 2026

1. Introduction

Baccharis trimera (Less.) DC. (Asteraceae family), commonly known as carqueja, is a medicinal plant native to South America. Traditional preparations of the aerial parts include typical infusion, tinctures, and dry extracts as a digestive, diuretic and for treating several diseases such as hepatic and gastric disorders (Ministério da Saúde, 2025; Silveira Rabelo and Caldeira Costa, 2018). In Brazil, *B. trimera* is officially recognized in the Brazilian Pharmacopeia, where the oral administration of preparations from its aerial parts are indicated for the treatment of dyspeptic symptoms (Fitoterapia Brasil, 2025). The species is also included in the National List of Medicinal Plants of Interest to the Unified Health System (RENISUS) and the Pharmacotherapeutic Formulary of the Brazilian Pharmacopeia (Antunes et al., 2024; Ministério da Saúde, 2025). Beyond its gastrointestinal indications, the aerial parts of *B. trimera* are traditionally used in Brazil to treat skin conditions, including skin wounds, ulcers, and inflammatory skin disorders (Castro, 2025; Silveira Rabelo and Caldeira Costa, 2018). Although the traditional use of *B. trimera* is not directly related to skin aging or pigmentation disorders, its metabolite profile includes flavonoids, phenylpropanoids, and terpenoids, which are classes of compounds with well-documented enzyme inhibitory and anti-inflammatory activities relevant to these endpoints. This phytochemical profile provides a rationale for expanding the pharmacological investigation of *B. trimera* to include potential cosmeceutical applications.

Skin aging is driven by several factors, including oxidative stress, pro-inflammatory mediators, and the overexpression of enzymes such as elastase and tyrosinase (Calleja-Agius et al., 2013). Elastase is a proteolytic enzyme belonging to the serine protease family, and its excessive hydrolytic activity contributes to a loss of skin elasticity while promoting inflammatory processes in cutaneous tissues (Korkmaz et al., 2010). Tyrosinase is an essential metalloenzyme in the melanogenesis pathway, catalyzing the oxidation of the substrates *L*-tyrosine and *L*-3, 4-dihydroxyphenylalanine (L-DOPA) (Ismaya et al., 2011; Videira et al., 2013). Excessive melanin production can lead to dermatological conditions such as melasma, age spots, and skin cancer (Brenner and Hearing, 2008; Unver et al., 2006). Most modern cosmetics with skin-lightning properties contain tyrosinase inhibitors (Pillaiyar et al., 2017). Consequently, elastase and tyrosinase are considered attractive molecular targets for cosmetic applications, and their inhibitors can be used as anti-wrinkle and skin-whitening agents, helping to delay skin aging and supporting the treatment of dermatological disorders (Chiocchio et al., 2018; Korkmaz et al., 2010; Videira et al., 2013).

Ethnopharmacological surveys and studies on medicinal plants used for skin disorders and cosmetic purposes have shown that traditional knowledge frequently guides the discovery of new cosmeceutical ingredients, especially those targeting inflammation, tissue repair, and pigmentation (Pieroni et al., 2004; Pranskuniene et al., 2022). An increasing use of raw materials derived from natural sources has been observed in recent years due to their advantageous properties, such as lower risk of allergic reactions and biodegradability (Silva et al., 2024). In this context, plant extracts are widely employed as sources of antioxidants, skin-whitening agents, anti-aging compounds, and anti-inflammatory agents, particularly for applications related to skin aging and dermatological disorders (Chiocchio et al., 2018; Koch et al., 2019; Lianza et al., 2020; Pillaiyar et al., 2017; Xue et al., 2017).

Phytochemical studies of *B. trimera* have revealed a rich metabolic profile including flavonoids (flavones and flavonols), sesquiterpenes, saponins, phenolic acids, monoterpenes, and diterpenes (Aboy et al., 2012; Borella et al., 2006; Caneschi et al., 2015; Duarte et al., 2005; Rodrigues et al., 2009; Silveira Rabelo and Caldeira Costa, 2018). Many of these metabolite classes are associated with anti-inflammatory, antioxidant, and enzyme-modulating activities that are relevant for skin protection and cosmeceutical applications. This particular species of *Baccharis* exhibits a broad range of pharmacological activities, including analgesic, antioxidant, anti-inflammatory, gastroprotective, hepatoprotective, antimicrobial, antifungal, antiparasitic, and weight-loss-promoting effects, among others (Da Cruz Padua et al., 2013; Dickel et al., 2007; Oliveira et al., 2012; Silveira Rabelo and Caldeira Costa, 2018). Although *B. trimera* has been investigated in different pharmacological contexts, its potential for skin-related applications remains poorly explored, particularly regarding enzyme inhibition associated with pigmentation and skin aging, as well as its anti-inflammatory activity in human macrophage-based in vitro models. Macrophages are key mediators of inflammation in wound healing. They are present in the dermis and subcutaneous tissue, where they play a central role in regulating inflammatory responses relevant to skin disorders (Koh and DiPietro, 2011). THP-1-derived macrophages are a well-established human cell model for evaluating the anti-inflammatory potential of plant-derived compounds in a standardized manner and represent an appropriate first-line screening model for assessing the capacity of extracts to modulate pro-inflammatory signaling pathways (Chanput et al., 2014). Therefore, this study evaluated the crude ethanolic extract and fractions of *B. trimera* for tyrosinase and elastase inhibitory activities, as well as their effects on modulation of inflammatory mediators in THP-1-derived macrophages. In addition, LC–HRMS-based dereplication of the crude extract and active fractions was performed to provide a preliminary overview of metabolites that may be associated with the observed bioactivities.

2. Materials and methods

2.1. Chemicals and reagents

Mushroom tyrosinase enzyme (EC 1.14.18.1), porcine pancreatic elastase enzyme (E.C.3.4.21.36), N-succinyl-Ala-Ala-Ala-p-nitroanilide ($sucAla_3$-pNA, S4760), *L*-3,4-dihydroxyphenylalanine (L-DOPA, D9628), kojic acid, quercetin hydrate ≥95% (337951), and trizma buffer were obtained from Sigma-Aldrich (San Luis, MO, USA). Anhydrous monobasic potassium phosphate buffer was purchased from Êxodo Científica (Sumaré, SP, Brazil).

2.2. General experimental procedures

All solvents used in the extraction and fractionation procedures were purchased from Dinâmica, Synth and Vetec (Indaiatuba, SP, Brazil). The LC-HRMS system was composed of a LC, 1290 Infinity II system (Agilent, Barueri, SP, Brazil), equipped with a high-resolution mass spectrometer (HRMS) with a quadrupole time-of-flight mass analyzer (QTOF, Impact HD) and electrospray ionization (ESI) source (Bruker Daltonics, Bremen, Germany) (FAPESP, 2014/50244-6). For the analysis of the fractions, an Orbitrap Exploris 240 mass spectrometer equipped with a heated electrospray ionization (ESI) interface and coupled to a Vanquish Flex HPLC system (Thermo Fisher Scientific, Waltham, MA, USA) was used. Enzymatic assays were performed at a spectrophotometer Cary 60 UV-Vis model G6860A (MY24239213) (Agilent Technologies, Santa Clara, CA, USA).

2.3. Plant material

Access to the genetic heritage was registered in SISGEN (https://sisgen.gov.br/) under code A9D0265. A voucher specimen of the species was deposited in the Herbarium of the Federal University of Goiás (no. 71186).

2.4. Extraction and sample preparation

An ethanolic extract from fresh leaves of *Baccharis trimera* was provided by Livealoe. The company's extraction procedure for fresh plants began with washing the harvested leaves with water, detergent, and 1% hypochlorite, followed by rinsing with potable water. The leaves were then placed on a tray for 30 min to remove excess moisture. A second

cleaning was carried out with 70% alcohol for 20 min. Subsequently, 4 kg of fresh leaves were blended with 96% ethanol, and the mixture was transferred to glass jars wrapped with non-woven fabric to protect it from light. The material was subjected to maceration for 30 min, and this procedure was repeated daily for 20 days. After the extraction period, the plant material was filtered. Solvent removal was performed at LaBiOrg (Laboratory of Biochemistry and Organic Chemistry, UFCAT) using a rotary evaporator under reduced pressure at 40 °C, yielding 124.1 g of crude ethanolic extract (*Bt*E; yield = 3.1%, based on fresh leaf weight). Fractionation of the crude extract (*Bt*E, 50 g) was carried out by liquid-liquid partitioning. The extract was initially suspended in methanol/water (3:7, v/v) and sequentially extracted with hexane (700 mL), dichloromethane (900 mL), and ethyl acetate (800 mL). Solvent removal under reduced pressure yielded 2.7 g of the hexane fraction (*Bt*EH; yield = 5.4%), 4.4 g of the dichloromethane fraction (*Bt*ED; yield = 8.7%), and 5.94 g of the ethyl acetate fraction (*Bt*EA; yield = 11.9%). In addition, 1.0 g of the hydroalcoholic fraction (*Bt*EHy; yield = 2.0%) was obtained after lyophilization. Fraction yields were calculated based on the weight of the crude extract.

The ethanolic extract (*Bt*E) and all fractions were stored at −20 °C until use.

2.5. LC-HRMS analysis

A stock solution of the crude extract *Bt*E was prepared by dissolving 5 mg of extract in 1 mL of water/methanol/isopropanol (4:3:3). For the analysis, the stock solution was diluted to 0.5 mg/mL in the same solvent mixture, and 1 µL was injected into the LC-HRMS system. Stock solutions of the derived fractions (*Bt*EH, *Bt*ED, *Bt*EA, and *Bt*EHy) were prepared at a concentration of 100 mg/mL in DMSO/ethanol (1:1) and sonicated in an ultrasonic bath for 10 min. The resulting solutions were filtered using a 0.22 µm nylon membrane filter and subsequently diluted to 10 mg/mL using methanol/water (8:2). A volume of 1 µL of each diluted solution was then injected into the LC-HRMS system.

Analysis of *Bt*E was performed using a linear gradient (ΔB 5-100%) over 20 min and a flow rate of 0.4 mL min^{-1} at 40 °C using a Cortecs™ C18+ analytical column (2.7 µm particle size; 100 × 2.1 mm; Waters, Milford, MA, USA). The mobile phase consisted of 0.1% formic acid in water (solvent A) and 0.1% formic acid in acetonitrile (solvent B).

Ionization experiments were conducted in positive ion mode $[M + H]^+$, with the following ESI source parameters: capillary voltage, 4500 V; quadrupole energy, 5 eV; collision cell energy, 5 eV; transfer time, 50 and 90 µs; pre-pulse time: 6 µs; nebulization pressure, 4 bar; drying gas flow, 8 L/min; and source temperature, 180 °C. Full-scan HRMS data were acquired over an *m/z* range of 100–1000. Data dependent MS/MS acquisition was performed in automatic mode with collision energies of 30 and 50 eV applied across the full *m/z* range. Compound identification from the crude extract was performed using Bruker Smart Formula 3D, CompoundCrawler and DataAnalysis 4.0 software (Bruker Daltonics, Bremen, Germany). The chromatographic conditions for fraction analysis were as follows: separation was performed on a Kinetex C18 column (50 × 2.1 mm, 2.6 µm, 100 Å, Phenomenex), using a gradient of 5–100% acetonitrile in water (both containing 0.1% formic acid) at a flow rate of 0.4 mL/min over 16 min, followed by 100% acetonitrile for 4 min.

HRMS data were acquired in both positive and negative ionization mode with ESI spray voltage 3.5 kV and −2.5 kV, respectively. The capillary temperature was set at 350 °C, the sheath gas flow rate at 40 L/min, and the auxiliary gas flow rate 5 L/min. Full-scan spectra were acquired from *m/z* 133.4 to 2000 at a resolution of 35,000 (at *m/z* 200), with an automatic gain control (AGC) 5 x 10^5 and a maximum injection time of 120 ms. MS/MS spectra were acquired in data-dependent acquisition mode (dd-MS^2), using stepped collision energies of 30, 60, and 75 eV (resulting in a normalized collision energy of 55 eV), a resolution of 17,500 (at *m/z* 200), an AGC of 2 x 10^5, and a maximum injection time of 75 ms. A TopN experiment (N = 5, loop count = 5) was implemented for triggering $ddMS^2$ acquisition.

2.6. MS/MS data processing

2.6.1. Crude extract data analysis

The standard protocol (https://ccms-ucsd.github.io/GNPSDocumentation/) available at the GNPS platform was used for MS/MS data treatment (Wang et al., 2016). Data processing included the following sequential steps (Da Mendes et al., 2023), converting experimental MS/MS data into.mzML (data files) by using the MSConvert software. Afterwards, the data were compressed by employing the program WinSCP client FTP and uploaded to the workflow at the GNPS platform (http://gnps.ucsd.edu) and Data Analysis 4.0 (Bruker Daltonics, Bremen, Germany). The data files deposited at the GNPS platform can be accessed at https://gnps.ucsd.edu/ProteoSAFe/status.jsp?task=f40344ef922244b48c3b88f14cb4a5ff.

After the spectral clustering algorithm (software MS-Cluster) was run, datasets were downloaded from GNPS pages into Cytoscape (version 3.10.1) together with MS/MS features. The clusters were constructed by product ion similarities joining the nodes by edges. For molecular networking the mass tolerance of 0.02 Da was used for both precursor peaks and the MS/MS fragment ions. The edges were filtered to have a cosine score above 0.7 and over six matched peaks. The bordering of molecular family was defined as 100. The network spectra were considered to match the library spectra when the score was above 0.7 and there were at least six matched peaks.

The product ion spectra were compared to the spectra available at free online compound screening libraries by using the software tools CompoundCrawler (https://massbank.eu/; http://mona.fiehnlab.ucdavis.edu/; https://metlin.scripps.edu), Data Analysis 4.0, and the GNPS platform (http://gnps.ucsd.edu) (Allard et al., 2017; Gonçalves Neto et al., 2020). SIRIUS (6.3.3) was also used as an additional tool following (Böcker et al., 2009; Dührkop et al., 2015, 2019, 2021; Kim et al., 2021; Ludwig et al., 2020) pre-processing using MZmine (version 4.8.5) (Schmid et al., 2023). In addition, annotated compounds were analyzed and compared to literature data to confirm annotation. All compounds were annotated at MSI Levels 2 and 2a. These levels correspond to putative identifications based on spectral library matching and literature data, without confirmation using authentic reference standards (Table 1*S*).

2.6.2. Fraction data analysis

Raw MS data files were converted to.mzML files and filtered by polarity to separate positive and negative ion mode scans using msConvert (ProteoWizard, version 3.0). Only the positive ion mode data were used for analyses. Raw data processing was performed using MZmine (version 4.19.4) utilizing several modules for feature processing, alignment, grouping, and ion identity networking. Additionally, a spectral library search was performed using open access spectral libraries, including MSnLib (https://doi.org/10.5281/zenodo.16984129), MassBank of

Table 1
Percentage of inhibition (%) of enzymes obtained from fractions and ethanolic extract of *B. trimera* (*Bt*E).

Extract	Inhibition (%) Tyrosinase (100 µg/mL)	Inhibition (%) Elastase (100 µg/mL)
*Bt*E	12 ± 2	30.4 ± 1.2
*Bt*EH	5.7 ± 0.7	No inhibition
*Bt*ED	69.7 ± 3.2	6.7 ± 0.5
*Bt*EA	65.3 ± 0.5	29.8 ± 2.2
*Bt*EHy	7.3 ± 0.5	17.6 ± 0.9
Kojic acid	86.5 ± 1.3	n.d.
Quercetin	n.d.	97.1 ± 2.6

*Bt*EH: hexane, *Bt*EA: ethyl acetate, *Bt*EHy: hydroalcoholic fractions; Quercetin (positive control of elastase), and Kojic acid (positive control for tyrosinase). nd: not determined.

North America, MassBankEU, and GNPS (ALL_GNPS_NO_PROPOGATED). The exact processing workflow is provided as an. mzbatch file in the supplementary information. Exported feature lists were annotated using SIRIUS (version 6.3.4) and its associated tools, including SIRIUS (Dührkop et al., 2019), ZODIAC (Ludwig et al., 2020), CSI:FingerID fingerprint prediction (Shen et al., 2014; Dührkop et al., 2015), CANOPUS (Dührkop et al., 2021), NPClassifier (Kim et al., 2021), and CSI:FingerID structure database search. Results were exported as.tsv files and merged with the feature quantification table created in MZmine. Features grouped by the MZmine modules metaCorrelate and ion identity networking were subsequently merged to harmonize annotations across different adducts and ion-source modifications. When multiple adducts or in-source fragments were annotated within the same feature group, the feature with the highest confidence score was selected, and its annotation was assigned to the remaining features in that group.

2.7. In vitro bioactivity assays

2.7.1. Culture of THP-1 cell line

The human monocytic leukemia cell line THP-1 (ACC 16) was obtained from the German Collection of Microorganisms and Cell Cultures GmbH, Braunschweig, Germany. Cells were cultured in RPMI 1640 medium with GlutaMAX (Gibco, New York, USA) and supplemented with 10% fetal bovine serum (Bio&Sell, Feucht, Germany) in T-75 flasks in a humidified incubator at 37 °C and 5% CO_2. Subculturing was performed twice a week to maintain cell density within the recommended range of $1x10^5$ to $1x10^6$ cells/mL. Cultures were periodically tested for the absence of mycoplasma contamination using a Polymerase Chain Reaction based mycoplasma detection kit (Applied Biological Materials, Richmond, Canada).

2.7.2. THP-1 macrophage pro-inflammatory response assay

To achieve differentiation of THP-1 cells, 2×10^5 cells were seeded in each well of a 48-well multiwell plate in complete media supplemented with 50 ng/mL Phorbol 12-myristate 13-acetate (PMA) (Sigma Aldrich, Germany). After 48 h of incubation, the media was aspirated and the cells were gently washed three times with DPBS, followed by 24 h of incubation in complete media without PMA. Cells were treated with different concentrations of plant extracts, vehicle control, 0.5 μM dexamethasone as positive control and full media as negative control. After 1 h of pre-treatment, 100 ng/mL LPS from *E. coli* O111:B4 (Sigma Aldrich, Germany) was added from a stock solution. Samples for cytokine determination and LDH assay (Cytotoxicity Detection Kit LDH, Roche Diagnostics, Mannheim, Germany) were collected from the culture supernatants after 4 h (TNF-α) and 24 h (IL-6, IL-1β, LDH), centrifuged and cytokine samples were stored at −70 °C until analysis. After removal of all supernatants, 200 μL of media containing 0.5 mM WST-8 (Abcr Germany) and 40 μM Menadione (Sigma Aldrich, Germany) was added to each well. The plate was then incubated for 1 h before absorbance measurement using a microplate reader at 450 nm with a reference wavelength of 600 nm. One well containing no cells was used as a blank and its value was then subtracted from all values. LDH assay was performed using 100 μL supernatant from each well according to the manufacturer's instructions. Wells without LPS addition were used as low control while 50 μg/mL Digitonin (Carl Roth, Germany) was used as high control to calculate percent Cytotoxicity. For both assays values were normalized to the untreated control (LPS+) of each assay plate and represent viability and cytotoxicity respectively. Each assay plate contained three technical replicates for LPS + control and experimental conditions. For vehicle control, dexamethasone, Digitonin and LPS- two technical replicates were performed on each 48-well plate.

2.7.3. Determination of cytokine secretion

Cytokine concentrations in the supernatant were determined using commercially available ELISA kits for TNF-α, IL-1β, and IL-6 (Invitrogen, Life Technologies). All samples and standards were tested in duplicate according to the manufacturer's instructions. Signals below the lower limit of quantification (LLOQ) were assigned a value of zero. Values were normalized to the LPS + control of each assay plate.

2.7.4. Elastase inhibitory assay

Samples (extracts and fractions) were tested at a concentration of 100 μg/mL (1.6% DMSO:water). A 10 μL aliquot of each sample was added to the enzyme solution in a 96-well plate containing 280 μL of Trizma buffer (85 mM, pH 8.0), 10 μL of elastase solution (0.2 μg/mL). After 15 min of incubation at room temperature, 20 μL of the chromogenic substrate *N*-succinyl-Ala-Ala-Ala-*p*-nitroanilide (Suc-Ala_3-*p*NA, 0.3 mM) was added to initiate the reaction. Assays were performed in triplicate and included the following controls: blank (buffer with 1.6% DMSO), negative control (buffer, 1.6% DMSO, and enzyme solution), sample control (buffer and extract or fraction), and positive control (buffer, quercetin, and enzyme solution). Absorbance at 410 nm was monitored after 15 min using a UV–Vis spectrophotometer, according to previously established procedure (Chiocchio et al., 2018; Da Silva et al., 2025). Enzyme inhibition was calculated using Eq. (1): Inhibition (%) = 100 – {100 ×[(Af – Ai)/(Afc – Aic)]}, where A_i and A_f represent the absorbance values of the sample containing the extract/fraction and sample control, respectively, and A_{ic} and A_{fc} correspond to the absorbance values of the negative control and blank, respectively.

2.7.5. Tyrosinase inhibitory assay

The tyrosinase inhibitory activity of the extracts and fractions was evaluated using a spectrophotometric method with L-DOPA as the substrate, following previously described protocols (Da Silva et al., 2025; Hwang and Lee, 2007; Kanlayavattanakul et al., 2018). An enzyme solution (tyrosinase, 30 U/mL in 20 mM phosphate buffer, pH 6.5, 18 μL) was added to a 96-well plate containing the sample solutions at a concentration of 100 μg/mL (124 μL phosphate buffer, 113.6 μL ultrapure water, and 10 μL sample). The assay was performed in triplicate and included the following controls: blank (buffer and 1.6% DMSO), negative control (buffer, 1.6% DMSO, and tyrosinase solution), sample control (buffer and sample solution), and positive control (buffer, kojic acid, and tyrosinase solution). After incubation for 30 min at room temperature, 44.4 μL of L-DOPA (final concentration: 0.5 mM) was added to each well before analysis. Absorbance at 475 nm was monitored after 5 min at room temperature. Enzyme inhibition was calculated using Eq. (1), as described for the elastase inhibitory assay.

For IC_{50} determination, the procedure described above was followed using a serial dilution of the active fractions *Bt*ED and *Bt*EA, ranging from 15.7 μg/mL to 1000 μg/mL. The IC_{50} values were determined by fitting the inhibition data to a two-parameter sigmoidal equation, with the lower and upper asymptotes fixed at 0 and 100, respectively, after background correction. The equation used, $y = \frac{100}{1+(x/IC_{50})^s}$, assumes that y represents the percentage inhibition, x the concentration, and s the slope factor. This model assumes that y decreases as x increases. Data are expressed as the mean of three independent assays. Curve fitting and data analysis were performed using GraFit® software (version 5.0.13, Erithacus Software, United Kingdom).

2.8. Statistical analysis

Statistical analyses were performed using GraphPad Prism 10. For cell-based assays, group differences were evaluated using the Brown-Forsythe and Welch ANOVA test corrected for multiple comparisons using the Dunnett T3 test.

3. Results and discussion

3.1. Enzyme inhibition

The crude extract showed low tyrosinase inhibition at 100 μg/mL, however, after fractionation, the dichloromethane (*Bt*ED) and ethyl acetate fraction (*Bt*EA) showed 69.7% and 65.3% anti-tyrosinase activity, respectively (Table 1). In elastase assays *Bt*E showed 30.4% inhibition, while its fractions did not enhance the inhibitory potential. A previous study reported 82.9% elastase inhibition for a 100% ethanolic extract of *B. trimera* at a concentration of 1 mg/mL (Song et al., 2023). This inhibitory potential was attributed to the metabolites luteolin and caffeic acid, which exhibited 37.4% and 65.8% inhibition, respectively, at 250 μg/mL (Song et al., 2023).

The IC_{50} values were determined for the fractions with anti-tyrosinase activity *Bt*ED and *Bt*EA, revealing potencies of 41.2 ± 3.7 μg/mL and 132.8 ± 18.4 μg/mL, respectively. The ethyl acetate fraction reached a maximal inhibition of approximately 70%. The plateau observed in the dose-response curve may be related to a saturation effect or interference from compounds within the complex mixture at higher concentrations. Previous screening of 33 extracts of Cerrado plant species identified *Stryphnodendron adstringens*, *Pouteria torta* and *Eugenia dysenterica* as the most active extracts against tyrosinase, with IC_{50} values below ≤48.45 μg/mL (Zolghadri et al., 2019). Thus, *Bt*ED exhibited strong tyrosinase inhibitory activity, whereas *Bt*EA showed moderate activity compared with the positive control, kojic acid (IC_{50} = 13.14 μg/mL), and the other previously evaluated extracts (Zolghadri et al., 2019).

3.2. Cytotoxicity and anti-inflammatory activity

Anti-inflammatory activity was evaluated using PMA-differentiated THP-1 cells stimulated with LPS following pretreatment with different concentrations of crude extracts and fractions. Since plant extracts and fractions may affect cell viability, potentially causing non-specific changes in cytokine secretion, cell viability and cytotoxicity were determined in parallel using the WST-8 and LDH assays, respectively. Digitonin was used as a positive control for both cytotoxicity readouts: it causes necrotic cell lysis, resulting in drastically reduced metabolic activity (WST-8) and maximum LDH release due to membrane disruption. LPS treated cells showed an increase in LDH release indicating inflammatory cell death under our experimental conditions, thus all data points were normalized to the LPS control of each assay plate.

The crude extract (*Bt*E) significantly reduced viability in the WST-8 assay at 100 μg/mL ($p < 0.0001$), yet none of the derived fractions showed a reduction in viability (Fig. 1). *Bt*E exhibited only a slight and non-significant increase in LDH release compared to the vehicle control despite the nearly complete loss of the WST-8 signal. This discrepancy between the two cytotoxicity readouts suggests that *Bt*E does not induce classical necrotic cell death at this concentration because lytic necrosis would produce a proportional increase in LDH release (Filipova et al., 2018). The mechanism underlying the reduction in WST-8 remains unclear and could reflect interference with mitochondrial dehydrogenase activity, non-lytic cell cycle arrest, or an alternative form of cell death. Further experiments are required to distinguish between these possibilities.

*Bt*ED and *Bt*EH significantly reduced LDH release relative to the LPS + control. This finding is consistent with their cytokine-inhibitory activity and suggests attenuation of LPS-induced inflammatory cell death. LPS stimulation triggers inflammatory cell death in macrophages, measurable by LDH release (Kang et al., 2022; Rayamajhi et al., 2013). The reduction observed here may therefore reflect a broader anti-inflammatory effect of these fractions, although the specific mechanism was not investigated. In addition to cytokine quantification, LDH release may serve as a complementary readout for anti-inflammatory activity in macrophage-based assays.

Upon stimulation with LPS, THP-1-derived macrophages showed an increase in secretion of the pro-inflammatory cytokines TNF-α, IL-1β and IL-6. Dexamethasone, a common anti-inflammatory drug, was used as a positive control and significantly inhibited the secretion of all three cytokines (Fig. 2). To contextualize the normalized data, mean ± SD absolute cytokine concentrations in LPS-stimulated cells were 4973.3 ± 970.0 pg/mL for TNF-α, 89.1 ± 23.5 pg/mL for IL-1β, and 15.0 ± 4.5 pg/mL for IL-6. Dexamethasone (0.5 μM) treatment reduced

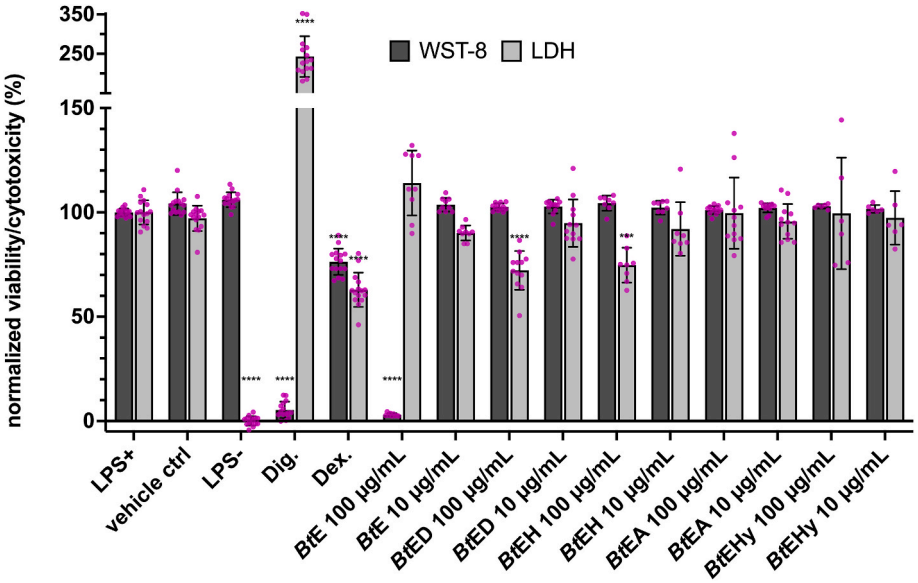

Fig. 1. Viability and Cytotoxicity of THP-1 macrophages in response to crude extract and fractions of *Baccharis trimera* determined by WST-8 and LDH assay, respectively. Data were normalized to the LPS + control of each assay plate and bars represent means ± SD from at least 3 independent biological experiments (3 technical replicates each, minimum n = 9 per condition); individual dots represent technical replicates. Dex. = 0.5 μM Dexamethasone; Dig. = 50 μg/mL Digitonin. *$p < 0.05$, **$p < 0.01$, ***$p < 0.001$, ****$p < 0.0001$ compared to the vehicle control as determined using Brown-Forsythe and Welch ANOVA test corrected for multiple comparisons using Dunnett T3 test. (For interpretation of the references to colour in this figure legend, the reader is referred to the Web version of this article.)

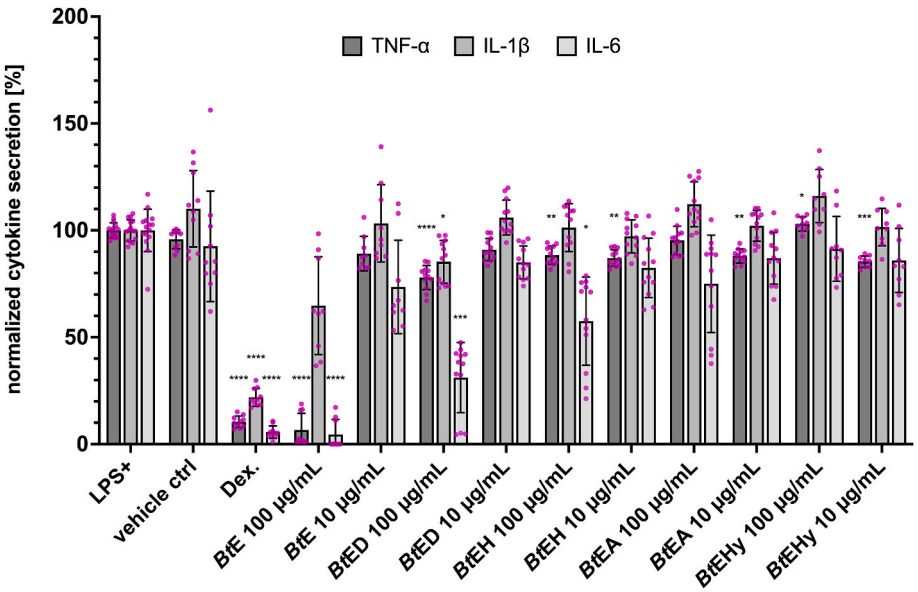

Fig. 2. Cytokine secretion of THP-1 macrophages in response to crude extract and fractions of *Baccharis trimera* determined by ELISA. Data were normalized to the LPS + control of each assay plate and bars represent means ± SD from at least 3 independent biological experiments (3 technical replicates each, minimum n = 9 per condition); individual dots represent technical replicates. Dex. = 0.5 µM Dexamethasone; Dig. = 50 µg/mL Digitonin. *p < 0.05, **p < 0.01, ***p < 0.001, ****p < 0.0001 compared to the vehicle control as determined using Brown-Forsythe and Welch ANOVA test corrected for multiple comparisons using Dunnett T3 test. (For interpretation of the references to colour in this figure legend, the reader is referred to the Web version of this article.)

TNF-α, IL-1β, and IL-6 to 536.7 ± 232.6 pg/mL, 19.6 ± 6.7 pg/mL, and 0.5 ± 0.3 pg/mL, respectively. *Bt*E showed significant reduction of two cytokines, highlighting the importance of a parallel viability readout to rule out non-specific effects on cytokine secretion due to cytotoxicity. *Bt*ED significantly reduced all three tested cytokines at 100 µg/mL while *Bt*EH was able to significantly inhibit TNF-α and IL-6 at 100 µg/mL.

The active compounds were of moderate to low polarity, as they preferentially partitioned into the dichloromethane fraction rather than the hexane or ethyl acetate fractions. *Bt*ED was the only fraction that significantly inhibited IL-1β, suggesting the presence of compounds that selectively target upstream regulators of IL-1β maturation and secretion. Since IL-1β processing depends on inflammasome activation, these results warrant further investigation into the potential effects on the NOD-, LRR- and pyrin domain-containing protein (NLRP3) pathway (Nunes and Souza, 2013). However, since the present study did not assess inflammasome-specific markers, such as caspase-1 activity or gasdermin D cleavage, any association between the observed IL-1β modulation and NLRP3 activation remains speculative and would require pathway-specific experiments for confirmation.

Taken together, the cytokine and LDH data suggest that *Bt*ED exerts a broad inhibitory effect on LPS-induced inflammatory responses in THP-1-derived macrophages. The inhibition of TNF-α, IL-6, and IL-1β observed in this study is consistent with the traditional use of *B. trimera* for wound healing and inflammatory skin conditions, providing preliminary in vitro support for this ethnopharmacological application. Although this model does not fully replicate the complexity of the cutaneous microenvironment, macrophages play a key role in dermal and wound-related inflammation. Inhibiting TNF-α, IL-6 and IL-1β suggests interference with conserved pro-inflammatory pathways that are relevant to multiple cell types. However, these results represent preliminary evidence and cannot be extrapolated to clinical efficacy without further validation in more complex biological models. Further research in skin-relevant models, such as keratinocytes or dermal fibroblasts, is required to establish whether the activity observed here can be applied to a broader cosmeceutical context.

3.3. Dereplication of compounds from crude extract and active fractions

LC–HRMS and MS/MS data analysis of *Bt*E enabled the annotation of fourteen secondary metabolites: 4′,8-dihydroxy-6,7-dimethoxyflavone (**1**), isokaempferide (**2**), eupatorin (**3**), 5-hydroxy-3′,4′,6,7-tetramethoxyflavone (**4**), isoshaftoside (**5**), apigenin-6,8-di-*C*-hexoside (vicenin 2) (**6**), apigenin-8-*C*-hexoside (**7**), rutin (**8**), dicaffeoylquinic acid (**9**), octadecatrienoic acid (**10**) gibberellin A53 (**11**), annoglabasin C (**12**), copalic acid (**13**) and 3-hydroxy-copalic acid (**14**) (Figs. 1S–19S; Table 1S).

Additionally, an untargeted investigation of the active fractions *Bt*ED and *Bt*EA was conducted to identify other compounds that may contribute to the observed biological activities. Among the dereplicated compounds, eight were annotated in both *Bt*E and active fractions (**1**, **3**–**6**, **9**, **11** and **13**), and six additional compounds were revealed in the active fractions: jaceosidin (**15**), 5,4′-dihydroxy-6,7,3′-trimethoxyflavone (cirsilineol) 4′-monoglucoside (**16**), 6-hydroxyluteolin 6,4′-dimethyl ether 7-rutinoside (**17**), 2,3-di(octadeca-9,12-dienoyloxy) propyl octadec-11-enoate (**18**), eugenyl *O*-β-apiofuranosyl-*O*-β-hexopyranoside (**19**), and eugenyl hexoside (**20**) (Figs. 20S–31S; Table 2S).

Compounds **1**–**10** were directly annotated by GNPS (Global Natural Products Social Molecular Networking) platform (http://gnps.ucsd.edu) (Allard et al., 2017; Da Mendes et al., 2023; Gonçalves Neto et al., 2020). The molecular networking analysis was further extended using SIRIUS (Böcker et al., 2009; Dührkop et al., 2015, 2019, 2021; Kim et al., 2021; Ludwig et al., 2020), resulting in the annotation of compounds **1**–**6** and **9**–**20**; however, alternative isomers were suggested for some compounds, such as hispidulin and chrysoeriol for compound **2** and vicenin 2 for compound **6** (Table 1S and Fig. 1S). Additionally, compounds (**1**–**14**) were manually dereplicated using the software tools CompoundCrawler (https://massbank.eu/; http://mona.fiehnlab.ucdavis.edu/; https://metlin.scripps.edu) and Data Analysis 4.0 (Bruker Daltonics, Bremen, Germany).

To facilitate the annotation of compounds and compound classes potentially associated with these activities, CANOPUS was used as an additional tool for the MS/MS data analysis of the fractions. CANOPUS is a computational tool that predicts compound classes for metabolite features based on their MS/MS spectra, enabling the classification of

metabolites detected in LC–HRMS experiments, even when their structures have not been previously reported or are not available in reference databases (Dührkop et al., 2021).

High resolution mass spectrometry data obtained in positive ESI ion mode $[M + H]^+$ were compared with literature data. This comparison, together with manual dereplication, enabled the differentiation of several isomer annotations (Abdel Ghani et al., 2023; Beelders et al., 2014; Colombo et al., 2008; Jan and Gavahian, 2024; Li et al., 2019; Raju et al., 2015; Razgonova et al., 2022; Satheeshkumar et al., 2014; Shawl et al., 1988; Wu et al., 2007).

The flavonoid **1** was assigned based on its molecular ion at *m/z* 315.0871($C_{17}H_{14}O_6$) and its characteristic product ions (Table 1S). Loss of two methoxy groups afforded the fragment ion at *m/z* 254.0577, which, after retro-Diels-Alder (RDA) fragmentation, produced the ion fragment at *m/z* 136.0159 and *m/z* 108.0209. This fragmentation pattern is consistent with a flavone bearing two methoxy groups and one hydroxy group on ring A, and one hydroxy group on ring B (Raju et al., 2015; Shawl et al., 1988). However, GNPS suggested a structure with ring B positioned at C-3, corresponding to 4′,5-dihydroxy-6,7-dimethoxyisoflavone (Fig. 1S). From a chemotaxonomic perspective, isoflavones are uncommon in the Asteraceae family, which further supports the flavone annotation (Sareedenchai and Zidorn, 2010). Subsequent spectral library matching in MZmine and *in-silico* structure prediction using SIRIUS consistently returned cirsimaritin (4′,5-dihydroxy-6,7-dimethoxyflavone) as the highest-scoring candidate (Table 2S; Fig. 26S). Although cirsimaritin was consistently annotated by multiple analytical tools, the position of hydroxy group on ring A cannot be unequivocally confirmed without orthogonal validation using an authentic reference standard. Consequently, the 4′,8-dihydroxy isomer cannot be fully excluded.

Dereplication of the other flavones (**2**–**7**) was performed using their protonated molecular ions $[M + H]^+$ at *m/z* 301.0707 ($C_{16}H_{12}O_6$), 345.0975 ($C_{18}H_{16}O_7$), 359.1125 ($C_{19}H_{18}O_7$), 565.1556 ($C_{26}H_{28}O_{14}$), 595.1656 ($C_{27}H_{30}O_{15}$), and 433.1115 ($C_{21}H_{20}O_{10}$), respectively, with fragment ions (Table 1S) compared to literature data. For compound **2,** the MS^2 spectrum displayed ions at *m/z* 258.0520 $[M + H - CH_3 - CO]^+$ and 229.0495 (RDA cleavage) (Razgonova et al., 2022), allowing differentiation from hispidulin and chrysoeriol (SIRIUS), in which methoxy group is located on rings A and B, respectively, whereas in isokaempferide it is located on ring C. Isokaempferide (**2**) has been previously identified in *Baccharis conferta* (Cortes-Morales et al., 2019).

For compound **3**, characteristic product ions appeared at *m/z* 284.0682 $[M + H - CO]^+$ derived from the precursor ion at *m/z* 312.0627, as well as at *m/z* 148.0522 (RDA cleavage in ring C of the flavonoid) (Li et al., 2019). The flavonoid **3** was assigned as eupatorin, as it has previously been identified in *B. trimera* and is recognized as a phytochemical marker of the genus *Baccharis* (Della Sahid et al., 2022; Verdi et al., 2005). The loss of methyl group and CO is a common fragmentation pathway in methoxylated flavonoids. For compound **4**, characteristic product ions were observed, including the B-ring RDA fragment at *m/z* 162.0677. Additionally, the ion at *m/z* 108.0206 was generated by the subsequent loss of CO_2 from the RDA fragment (Jan and Gavahian, 2024). Polymethoxylated flavonoids are very common in *Baccharis* spp. (Della Sahid et al., 2022).

For compound **5**, the MS^2 spectrum showed ions at *m/z* 379.0811 $[M + H - 186]^+$, 325.0702 $[M + H - 240]^+$ and 295.0601 $[M + H - 270]^+$, corresponding to further fragmentations of the sugar moieties (Colombo et al., 2008). This flavonoid was annotated as isoshaftoside and it has previously been identified in *B. trimera* by (Ximenes et al., 2022).

For compound **6**, the fragment ion at *m/z* 325.0699 $[M + H - C_{15}H_{10}O_5]^+$ represents the loss of the apigenin aglycone moiety. SIRIUS suggested vicenin 2, whereas GNPS annotation placed the hexose units at different positions on ring A, consistent with apigenin-5,7-di-*C*-hexoside (Beelders et al., 2014). Compound **7** showed fragment ions at *m/z* 416.1035 $[M + H - 17]^+$, 313.0696 $[M + H - 120]^+$, and the ion at *m/z* 284.0586 was generated by the loss of CHO (−29 Da) from the ion at *m/z* 313.0696 (Colombo et al., 2008). Apigenin *C*-hexoside derivatives have been reported in *B. trimera*, as well as compounds **5**, **6**, and **7**, and this class is considered as phytochemical marker of the genus *Baccharis* (Budel et al., 2018; Ximenes et al., 2022).

Flavonol **8** exhibited an $[M + H]^+$ ion at *m/z* 611.1632 ($C_{27}H_{30}O_{16}$) and showed a characteristic fragmentation pathway involving the loss of a hexoside and a methyl pentoside moiety, with ions at *m/z* 465.1021 (loss of $C_6H_{12}O_4$) and *m/z* 303.0500 (loss of $C_{12}H_{22}O_9$) (Satheeshkumar et al., 2014). The presence of a disaccharide rutinose moiety was suggested for compound **8**, since rutin has previously been identified in *B. trimera* (Sabir et al., 2017; Ximenes et al., 2022).

Compound **9** displayed a molecular ion at *m/z* 517.1346 ($C_{25}H_{24}O_{12}$) and product ions characteristic of dicaffeoylquinic acid, such as *m/z* 499.1237 $[M + H - 18]^+$, formed by water loss, and *m/z* 163.0392, associated with the presence of a caffeoyl unit. The ion at *m/z* 319.0809 was produced by the loss of caffeoyl acid from the fragment ion at *m/z* 499.1237 (Wu et al., 2007). Dicaffeoylquinic acids have previously been identified in *B. trimera* such as 3,4-, 3,5- and 4,5-dicaffeoylquinic acid (Ximenes et al., 2022) and 1,5-dicaffeoylquinic acid (cynarin) (Aboy et al., 2012).

Compound **10** is an octadecatrienoic acid annotated as linolenic acid ($C_{18}H_{30}O_2$) (Abdel Ghani et al., 2023) based on its protonated molecular ion at *m/z* 279.2314 and its MS^2 data, which included fragment ions at *m/z* 149.0241, 223.1689 $[M + H - 56]^+$ (loss of CO and rearrangement), and 261.2223 $[M + H - 18]^+$. Linolenic acid was previously identified in the seeds of *Baccharis dracunculifolia* (Morais and Castanha, 2011). A compound structurally related to linoleic acid (**19**), with a molecular ion at *m/z* 898.7856 ($C_{57}H_{100}O_6$), was annotated as 2,3-di(octadeca-9, 12-dienoyloxy) propyl octadec-11-enoate and detected in both active fractions, *Bt*EA and *Bt*ED. Although no previous reports of this exact structure were found, triacylglycerols containing linoleic acid moieties are widely distributed in seed and vegetative tissues of the Asteraceae family.

Among the annotated diterpenes, compound **11** was annotated as a gibberellin A53, a phytohormone typically present in plant tissues at trace levels. The molecular ion at *m/z* 349.2013 ($C_{20}H_{28}O_5$) was detected, along with fragment ions at *m/z* 331.1908 $[M + H - 18]^+$, 313.1805 $[M + H - 2H_2O]^+$, and 285.1853 $[M + H - 2H_2O - CO]^+$, consistent with the annotation of gibberellins (Frusciante et al., 2024). Compound **12** was annotated based on its molecular ion at *m/z* 407.2442 ($C_{23}H_{34}O_6$) and its corresponding fragment ions (Table 1S) (Chen et al., 2000). The *ent*-kaurane skeleton is a fundamental biosynthetic precursor in the gibberellin metabolic pathway and has been identified in *Baccharis ramosissima*, *Baccharis truncata* (Bohlmann et al., 1981), *Baccharis lateralis*, and *Baccharis retusa* (Silva et al., 2022).

Compounds **13** and **14** are labdane-type diterpenes previously identified in *Baccharis dracunculifolia* (Midorikawa et al., 2003) and are widely distributed among other *Baccharis* species (Martinez et al., 2005). These compounds were annotated based on their molecular ions at *m/z* 305.2470 ($C_{20}H_{32}O_2$) and *m/z* 321.2427 ($C_{20}H_{32}O_3$), respectively, along with their expected structural fragmentation patterns (Aguiar et al., 2018). Dehydration and decarboxylation pathways are consistent with labdane-type carboxylic acid diterpenes, as evidenced by fragment ions at *m/z* 287.2364 $[M + H - H_2O]^+$ and 269.2259 $[M + H - 2H_2O]^+$ for compound **13**, and *m/z* 303.2317 $[M + H - H_2O]^+$ and 285.2204 $[M + H - 2H_2O]^+$ for compound **14**.

Flavones with molecular ions at *m/z* 331.0813 ($C_{17}H_{14}O_7$), *m/z* 507.1497 ($C_{24}H_{26}O_{12}$), and 639.1916 ($C_{29}H_{34}O_{16}$), together with their characteristic product ions and comparison with literature data (Es-Safi et al., 2005; Song et al., 2009; Zhang et al., 2018), were annotated as jaceosidin (**15**), 5,4′-dihydroxy-6,7,3′-trimethoxyflavone (cirsilineol) 4′-monoglucoside (**16**) and 6-hydroxyluteolin 6,4′-dimethyl ether 7-rutinoside (**17**), respectively. The product ions at *m/z* 316.0569 $[M + H - CH_3]^+$, *m/z* 301.0349 $[M + H - 2CH_3]^+$, and *m/z* 168.0055 (RDA fragment) were observed for jaceosidin. For compound **16** and **17**, sequential sugar losses followed by characteristic fragmentation of the

methoxylated flavone skeleton were observed, consistent with the fragmentation behavior reported for 6-hydroxyluteolin glycosides (Es-Safi et al., 2005). This was evidenced by the fragment ions at *m/z* 345.0960 $[M + H - 162]^+$ and *m/z* 330.0721 $[M + H - CH_3]^+$ for compound **16**. Compound **16** was detected in both active fractions, whereas flavone **17** was annotated only in *Bt*EA and compound **15** only in *Bt*ED. Compound **16**, annotated as 5,4′-dihydroxy-6,7,3′-trimethoxy-flavone (cirsilineol) 4′-monoglucoside, has previously been reported in another genus of the Asteraceae family, *Cirsium*, specifically in *Cirsium lineare* (Morita et al., 1973). Although the structure of compound **17** has not been previously reported, flavones are widely distributed in *Baccharis* species, including structurally related derivatives (Budel et al., 2018; Ximenes et al., 2022). Notably, jaceosidin (**15**), previously isolated from *Baccharis grisebachii* and *Baccharis gaudichaudiana*, is recognized as a phytochemical marker of the genus (Ramos Campos et al., 2016).

The phenylpropanoids detected as ammoniated adducts, $[M + NH_4]^+$ at *m/z* 476.2124 ($C_{21}H_{30}O_{11}$) and *m/z* 344.1703 ($C_{16}H_{22}O_7$), were annotated as eugenyl *O*-β-apiofuranosyl-*O*-β-hexopyranoside (**19**) and eugenyl hexoside (**20**), respectively, and were present in both fractions. The characteristic fragmentation pattern of eugenol was observed (Salem et al., 2021), including the ion at *m/z* 165.0911 (Figs. 24S and 25S). Eugenyl glycoside (citrusin) has previously been isolated and characterized from the roots of *Lactuca virosa* (Asteraceae), whereas compound **20** has been reported in *Tinospora sinensis* (Menispermaceae) (Kisiel and Barszcz, 1997), a Chinese medicinal plant with recognized anti-inflammatory potential (Li et al., 2004).

Most of the annotated compounds have been reported to possess anti-inflammatory potential (**1**–**3**, **5**, **8**–**10**, and **12**–**15** and **20**) (Al-Dhabi et al., 2015; Almeida et al., 2021; Calder, 2017; Clavin et al., 2007; Da Kim et al., 2022; Guan et al., 2022; Laavola et al., 2012; Leal et al., 2009; Lee and Bae, 2016; Li et al., 2019; Serhan, 2014; Shin et al., 2017; Song et al., 2009; Verdi et al., 2005; Ximenes et al., 2022; Yang et al., 2022), which provides a plausible chemical rationale for the bioactivity observed for *Bt*ED and *Bt*EA. Cirsimaritin (**1**), one of the compounds enriched in *Bt*ED, has previously been shown to inhibit IL-6 and TNF-α secretion in LPS-stimulated RAW264.7 macrophages by acting upstream and suppressing NF-κB/IκBα signaling and STAT3 activation (Shin et al., 2017). Pharmacological studies have demonstrated the effectiveness of compound **2** in reducing acute inflammation in rodents, particularly in the carrageenan-induced paw edema model. A key cellular mechanism underlying this effect is its ability to directly inhibit myeloperoxidase activity in human neutrophils (Leal et al., 2009). In addition to these effects, compound **3** has demonstrated leishmanicidal activity against amastigotes, making it a promising candidate for the development of drugs targeting cutaneous leishmaniasis (Della Sahid et al., 2022). Its anti-inflammatory activity is mainly associated with the inhibition of inducible nitric oxide synthase (iNOS) and cyclooxygenase-2 (COX-2) expression, as well as the suppression of nitric oxide (NO), TNF-α, and prostaglandin E2 (PGE2) production (Laavola et al., 2012).

Similarly, isoshaftoside (**5**), a C-glycoside of apigenin, exhibits potent anti-inflammatory and immunomodulatory activity. This compound suppresses the production of pro-inflammatory mediators, including iNOS, TNF-α, IL-1β, and COX-2, thereby contributing to its anti-neuroinflammatory effects (Guan et al., 2022). In a comparable manner, the anti-inflammatory effect of rutin (**8**) has been attributed to its ability to inhibit the expression of COX-2 and inducible iNOS in ultraviolet B-irradiated mouse skin (Al-Dhabi et al., 2015), which may further contribute to the anti-inflammatory properties observed for *Bt*EA and *Bt*ED. Although there are no reports of anti-inflammatory activity for the other glycosylated flavonoids, compounds **16** and **17**, luteolin and its derivatives, such as luteolin-7-O-glucoside, have shown anti-inflammatory potential (Aziz et al., 2018; Wu et al., 2025).

Jaceosidin (flavone **15**), exclusively detected in the most active fraction *Bt*ED, has previously been reported to exhibit anti-inflammatory activity in the TPA induced mouse ear edema model. This effect has been associated with the inhibition of nitric oxide and prostaglandin E2 production, as well as suppression of cyclooxygenase-2 (COX-2) activity (Kim et al., 2008; Song et al., 2009). This flavone has also been reported to inhibit NF-kB activation and nitric oxide production in LPS-stimulated macrophages (Clavin et al., 2007; Song et al., 2009).

In a study investigating the anti-melanogenic effect of jaceosidin, the compound was not effective in primary human melanocytes and did not inhibit tyrosinase when evaluated at concentrations ranging from 5 to 30 μM, showing no influence on monophenolase activity (Goenka, 2025).

Additionally, a dicaffeoylquinic acid (**9**) was annotated in the extract and *Bt*EA. Notably, 1,5-dicaffeoylquinic acid (cynarin) has previously demonstrated the ability to reduce endothelial inflammation (Da Kim et al., 2022), suggesting that compounds of this class may also contribute to the biological activity observed.

Linolenic acid (**10**) is widely recognized for its role in modulating inflammatory responses and serves as a metabolic precursor for the synthesis of long-chain fatty acids, including eicosapentaenoic acid (EPA) and docosahexaenoic acid (DHA). These fatty acids are subsequently converted into bioactive lipid mediators that inhibit inflammation, promote neutrophil clearance, facilitate the removal of cellular debris, and restore tissue homeostasis, constituting a highly effective anti-inflammatory mechanism (Calder, 2017; Serhan, 2014).

In addition to phenolic and fatty acid derivatives, diterpenoids containing the *ent*-kaurane skeleton, such as compound **12**, also exhibit potent immunomodulatory activity. Mechanistically, these compounds act by inhibiting the synthesis of key pro-inflammatory mediators, particularly through the suppression of NF-kB-inducing kinase (NIK) (Castrillo et al., 2001). Compounds analogous to annoglabasin C (**12**), which share the *ent*-kaurane skeleton, were previously isolated from *Annona glabra* fruits and shown to inhibit NO production in LPS-stimulated RAW264.7 macrophages (Nhiem et al., 2015).

Copalic acid (**13**) and its derivative, compound **14**, are well known for their pharmacological potential, including notable anti-inflammatory effects (Medeiros et al., 2021; Souza et al., 2020).

Eugenyl hexoside (**20**), also known as citrusin, was detected in both *Bt*ED and *Bt*EA. Previous studies have reported anti-inflammatory activity for this compound, including significant inhibition of LPS-induced nitric oxide production in RAW 264.7 macrophages (Xu et al., 2022), suggesting that its presence in the active fractions may contribute to their observed anti-inflammatory effects.

Among the compounds dereplicated from *Bt*E, *Bt*ED, and *Bt*EA, several bioactive metabolites with anti-inflammatory potential were annotated in both the crude extract and the active fractions, including cirsimaritin (**1**) eupatorin (**3**), isoshaftoside (**5**), dicaffeoylquinic acid (**9**), and copalic acid (**13**), which may contribute to the observed biological activity. In addition, following extract fractionation, other bioactive compounds were annotated. Cirsimaritin (**1**), eupatorin (**3**) and jaceosidin (**15**), annotated exclusively in *Bt*ED, and citrusin (**20**), annotated in both *Bt*ED and *Bt*EA, are well-documented anti-inflammatory agents. Their presence may be associated with the enhanced anti-inflammatory activity observed in the fractions, particularly in *Bt*ED. Assessment of the relative distribution of annotated metabolites using SIRIUS CSI:FingerID and CANOPUS revealed differences among the fractions, with active fractions showing a greater representation of bioactive compound classes (Table S2). However, these findings should not be interpreted as quantitative evidence of metabolite enrichment, as MS signal intensities are affected by multiple factors, including ionization efficiency and matrix effects. Confirmation of differences in metabolite abundance will require targeted quantitative analyses using authentic standards.

Using the results obtained from NPClassifier, the relative composition of metabolite chemical classes was calculated for the crude extracts and fractions. This analysis showed that the most representative classes in the active fractions *Bt*EA and *Bt*ED were diterpenoids and flavonoids,

with phenylpropanoids representing an additional major class in *Bt*EA (Table S3). Diterpenoids and flavonoids are classes of secondary metabolites widely recognized for their anti-inflammatory potential (Al-Khayri et al., 2022; Ge et al., 2022). Therefore, their annotation in the active fractions is noteworthy and consistent with the more pronounced anti-inflammatory activity observed in these fractions.

Beyond anti-inflammatory properties, several compounds annotated in the extract are also associated with enzyme inhibitory activities. Numerous flavonoids, for example, are known to exhibit anti-elastase activity. Apigenin 6-*C*-glucoside showed an IC_{50} of 4.34 μM, demonstrating greater inhibitory potency than its aglycone against elastase (Jakimiuk et al., 2021). Therefore, the presence of compound **6** may contribute to the anti-elastase activity observed in the *Bt*E extract (Jakimiuk et al., 2021). Although the crude extract did not exhibit pronounced anti-tyrosinase activity, the fractions *Bt*ED and *Bt*EA demonstrated inhibitory potential, which may be associated with a higher concentration of active compounds after fractionation. For instance, vitexin (**7**), an apigenin flavone glucoside, and rutin (**8**), both annotated in *Bt*E, have previously shown IC_{50} values of 0.35 mM and 57.98 μM, respectively, in tyrosinase inhibition assays (Karaoğlan and Koca, 2020; Kim and Kang, 2015; Zhang et al., 2021). Additionally, 3-hydroxy-copalic acid (**14**) has been reported to inhibit tyrosinase activity, achieving 64% ± 1.5% inhibition at a concentration of 250 μM (Souza Vargas et al., 2015).

4. Conclusions

Baccharis trimera is a medicinal species of recognized ethnopharmacological relevance in Brazil and remains a valuable source of bioactive metabolites. In the present study, the crude ethanolic extract and its fractions were evaluated for in vitro skin-related bioactivities, and the dichloromethane fraction displayed the most consistent profile, combining marked tyrosinase inhibition with significant reduction in TNF-α, IL-1β, and IL-6 secretion, as well as decreased LPS-induced LDH release in THP-1-derived macrophages.

LC–HRMS-based dereplication of the crude extract and active fractions enabled the annotation of twenty metabolites, including flavonoids, hydroxycinnamic acid derivatives, diterpenes, phenylpropanoids, and fatty acids, several of which have previously been associated with anti-inflammatory or enzyme-inhibitory activities. These annotations provide a preliminary chemical basis for the observed bioactivities. In particular, the metabolites with anti-inflammatory potential annotated after fractionation, especially cirsimaritin, eupatorin and jaceosidin, which were exclusively annotated in the dichloromethane fraction, may help explain the pronounced enhancement in anti-inflammatory activity observed in this fraction.

Overall, the results indicate that fractionation strongly influences the bioactivity profile of *B. trimera* extracts and that medium-to low-polarity fractions deserve further investigation. The anti-tyrosinase activity observed for *Bt*ED and *Bt*EA represents a relevant finding for future studies on cosmetic and skin-related applications.

CRediT authorship contribution statement

Philipp Gabor: Formal analysis, Investigation, Methodology, Visualization, Writing – original draft. **Wéldion G. Mesquita Júnior:** Investigation, Writing – original draft. **Kyuri Ribeiro:** Investigation. **Romário Pereira da Costa:** Methodology, Writing – review & editing. **Quezia B. Cass:** Methodology, Writing – review & editing. **Vanessa Gisele Pasqualotto Severino:** Writing – review & editing. **Richele P. Severino:** Writing – review & editing. **Geísa Ferreira Costa Makishi:** Investigation. **Gislane Florambel Siqueira:** Investigation. **Matthias F. Melzig:** Conceptualization, Resources, Supervision, Writing – review & editing. **Alexander Weng:** Conceptualization, Resources, Supervision, Writing – review & editing. **Lorena R.F. de Sousa:** Conceptualization, Project administration, Resources, Supervision, Visualization, Writing – review & editing.

Declaration of competing interest

The authors declare that they have no known competing financial interests or personal relationships that could have appeared to influence the work reported in this paper.

Acknowledgments

This study was financially supported by the National Council for Scientific and Technological Development (CNPq) (Process 403611/2020-2, MAI/DAI Program at UFCAT), Goiás State Research Support Foundation (FAPEG, 202310267001406), and Study and Project Financing Agency (FINEP, 0558/21), Brazil. The authors also thank Livealoe Company for financial support.

Appendix A. Supplementary data

Supplementary data to this article can be found online at https://doi.org/10.1016/j.jep.2026.122117.

Abbreviations

LC–HRMS	liquid chromatography-high resolution mass spectrometry
LPS	lipopolysaccharide
LDH	lactate dehydrogenase
L-DOPA	*L*-3,4-dihydroxyphenylalanine
HRMS	high resolution mass spectrometry
ESI	electrospray ionization
AGC	automatic gain control
dd-MS^2	data-dependent acquisition mode
*Bt*E	*Baccharis trimera* ethanolic extract
*Bt*EH	*Baccharis trimera* hexane fraction
*Bt*ED	*Baccharis trimera* dichloromethane fraction
*Bt*EA	*Baccharis trimera* ethyl acetate fraction
*Bt*EHy	*Baccharis trimera* hydroalcoholic fraction
PMA	Phorbol 12-myristate 13-acetate
NLRP3	NOD-, LRR- and pyrin domain-containing protein 3
NF-κB	nuclear factor kappa B
RDA	retro-Diels-Alder
iNOS	inducible nitric oxide synthase
COX-2	cyclooxygenase-2
NO	nitric oxide
PGE2	prostaglandin E2
NIK	NF-kB-inducing kinase
EPA	eicosapentaenoic acid
DHA	docosahexaenoic acid
RENISUS	Medicinal Plants of Interest to the Unified Health System
SISGEN	National System for the Management of Genetic Heritage and Associated Traditional Knowledge
sucAla$_3$-*p*NA	N-succinyl-Ala-Ala-Ala-*p*-nitroanilide
THP-1	human monocytic leukemia cell line
TNF-α	tumor necrosis factor alpha
IL-6	interleukin 6
IL-1β	interleukin 1β
WST-8	water-soluble tetrazolium-8
DPBS	Dulbecco's phosphate-buffered saline
DMSO	dimethyl sulfoxide

Data availability

The data used in this study can be obtained from the corresponding authors upon submission of a reasonable request. The data files deposited at the GNPS platform can be accessed at https://gnps.ucsd.edu/ProteoSAFe/status.jsp?

task=f40344ef922244b48c3b88f14cb4a5ff.

References

Abdel Ghani, A.E., Al-Saleem, M.S.M., Abdel-Mageed, W.M., AbouZeid, E.M., Mahmoud, M.Y., Abdallah, R.H., 2023. UPLC-ESI-MS/MS profiling and cytotoxic, antioxidant, anti-inflammatory, antidiabetic, and antiobesity activities of the non-polar fractions of *Salvia hispanica* L. aerial parts. Plants 12, 1062. https://doi.org/10.3390/plants12051062.

Aboy, A.L., Apel, M.A., Debenedetti, S., Francescato, L., Rosella, M.A., Henriques, A.T., 2012. Assay of caffeoylquinic acids in *Baccharis trimera* by reversed-phase liquid chromatography. J. Chromatogr. A 1219, 147–153. https://doi.org/10.1016/j.chroma.2011.11.042.

Aguiar, G.P., Crevelin, E.J., Dias, H.J., Ambrósio, S.R., Bastos, J.K., Heleno, V.C.G., Vessecchi, R., Crotti, A.E.M., 2018. Electrospray ionization tandem mass spectrometry of labdane-type acid diterpenes. J. Mass Spectrom. 53, 1086–1096. https://doi.org/10.1002/jms.4284.

Al-Dhabi, N.A., Arasu, M.V., Park, C.H., Park, S.U., 2015. An up-to-date review of rutin and its biological and pharmacological activities. EXCLI J. 14, 59–63. https://doi.org/10.17179/excli2014-663.

Al-Khayri, J.M., Sahana, G.R., Nagella, P., Joseph, B.V., Alessa, F.M., Al-Mssallem, M.Q., 2022. Flavonoids as potential anti-inflammatory molecules: a review. Molecules 27, 2901. https://doi.org/10.3390/molecules27092901.

Allard, P.M., Genta-Jouve, G., Wolfender, J.L., 2017. Deep metabolome annotation in natural products research: towards a virtuous cycle in metabolite identification. Curr. Opin. Chem. Biol. 36, 40–49. https://doi.org/10.1016/j.cbpa.2016.12.022.

Almeida, N.S. de, Ferraz, A.d.B.F., Pedron, C., Correa, D.S., Vieira, L.B., Antunes, F.T.T., Souza, A.H. de, 2021. *Baccharis trimera* aqueous extract modulates inflammation and nociception in mice. Clin. Phytosci. 7, 82. https://doi.org/10.1186/s40816-021-00309-w.

Antunes, K.A., Raman, V., Perera, W.H., Heiden, G., Pontarolo, R., Farago, P.V., Khan, I. A., Manfron, J., 2024. Authentication and quality control of the Brazilian traditional herb 'Carquejas' (*Baccharis* species) using morpho-anatomy and microscopy. Plants 13, 3030. https://doi.org/10.3390/plants13213030.

Aziz, N., Kim, M.Y., Cho, J.Y., 2018. Anti-inflammatory effects of luteolin: a review of in vitro, in vivo, and in silico studies. J. Ethnopharmacol. 225, 342–358. https://doi.org/10.1016/j.jep.2018.05.019.

Böcker, S., Letzel, M.C., Lipták, Z., Pervukhin, A., 2009. SIRIUS: decomposing isotope patterns for metabolite identification. Bioinformatics 25, 218–224. https://doi.org/10.1093/bioinformatics/btn603.

Beelders, T., Beer, D. de, Stander, M.A., Joubert, E., 2014. Comprehensive phenolic profiling of *Cyclopia genistoides* (L.) Vent. by LC-DAD-MS and -MS/MS reveals novel xanthone and benzophenone constituents. Molecules 19, 11760–11790. https://doi.org/10.3390/molecules190811760.

Bohlmann, F., Kramp, W., Grenz, M., Robinson, H., King, R.M., 1981. Diterpenes from *Baccharis* species. Phytochemistry 20, 1907–1913. https://doi.org/10.1016/0031-9422(81)84033-2.

Borella, J.C., Duarte, D.P., Novaretti, A.A., Menezes, Jr. A., França, S.C., Rufato, C.B., Santos, P.A., Veneziani, R.C., Lopes, N.P., 2006. Variabilidade sazonal do teor de saponinas de *Baccharis trimera* (Less.) DC (Carqueja) e isolamento de flavona. Revista Brasileira de Farmacognosia 16, 557–561. https://doi.org/10.1590/s0102-695x2006000400020.

Brenner, M., Hearing, V.J., 2008. The protective role of melanin against UV damage in human skin. Photochem. Photobiol. 84, 539–549. https://doi.org/10.1111/j.1751-1097.2007.00226.x.

Budel, J.M., Wang, M., Raman, V., Zhao, J., Khan, S.I., Rehman, J.U., Techen, N., Tekwani, B., Monteiro, L.M., Heiden, G., Takeda, I.J.M., Farago, P.V., Khan, I.A., 2018. Essential oils of five *baccharis* species: investigations on the chemical composition and biological activities. Molecules 23, 2620. https://doi.org/10.3390/molecules23102620.

Calder, P.C., 2017. Omega-3 fatty acids and inflammatory processes: from molecules to man. Biochem. Soc. Trans. 45, 1105–1115. https://doi.org/10.1042/BST20160474.

Calleja-Agius, J., Brincat, M., Borg, M., 2013. Skin connective tissue and ageing. Best Pract. Res. Clin. Obstet. Gynaecol. 27, 727–740. https://doi.org/10.1016/j.bpobgyn.2013.06.004.

Caneschi, C.A., Martins, F.J., Larrudé, D.G., Romani, E.C., Brandão, M.A., Raposo, N.R., 2015. In vitro antifungal activity of *Baccharis trimera* less (DC) essential oil against dermatophytes. Trop. J. Pharmaceut. Res. 14, 2083. https://doi.org/10.4314/tjpr.v14i11.19.

Castrillo, A., Las Heras, B. de, Hortelano, S., Rodriguez, B., Villar, A., Bosca, L., 2001. Inhibition of the nuclear factor kappa B (NF-kappa B) pathway by tetracyclic kaurene diterpenes in macrophages. Specific effects on NF-kappa B-inducing kinase activity and on the coordinate activation of ERK and p38 MAPK. J. Biol. Chem. 276, 15854–15860. https://doi.org/10.1074/jbc.M100010200.

Castro, H.G. de, 2025. Contribuição ao estudo das plantas medicinais: carqueja (*Baccharis* spp.). Atena Editora.

Chanput, W., Mes, J.J., Wichers, H.J., 2014. THP-1 cell line: an in vitro cell model for immune modulation approach. Int. Immunopharmacol. 23, 37–45. https://doi.org/10.1016/j.intimp.2014.08.002.

Chen, C.Y., Chang, F.R., Cho, C.P., Wu, Y.C., 2000. Ent-kaurane diterpenoids from *Annona glabra*. J. Nat. Prod. 63, 1000–1003. https://doi.org/10.1021/np0000320.

Chiocchio, I., Mandrone, M., Sanna, C., Maxia, A., Tacchini, M., Poli, F., 2018. Screening of a hundred plant extracts as tyrosinase and elastase inhibitors, two enzymatic targets of cosmetic interest. Ind. Crop. Prod. 122, 498–505. https://doi.org/10.1016/j.indcrop.2018.06.029.

Clavin, M., Gorzalczany, S., Macho, A., Muñoz, E., Ferraro, G., Acevedo, C., Martino, V., 2007. Anti-inflammatory activity of flavonoids from Eupatorium arnottianum. J. Ethnopharmacol. 112, 585–589. https://doi.org/10.1016/j.jep.2007.04.007.

Colombo, R., Yariwake, J.H., McCullagh, M., 2008. Study of *C*- and *O*-glycosylflavones in sugarcane extracts using liquid chromatography: exact mass measurement mass spectrometry. J. Braz. Chem. Soc. 19, 483–490. https://doi.org/10.1590/s0103-50532008000300016.

Cortes-Morales, J.A., Olmedo-Juárez, A., Trejo-Tapia, G., González-Cortazar, M., Domínguez-Mendoza, B.E., Mendoza-de Gives, P., Zamilpa, A., 2019. In vitro ovicidal activity of *Baccharis conferta* Kunth against Haemonchus contortus. Exp. Parasitol. 197, 20–28. https://doi.org/10.1016/j.exppara.2019.01.003.

Da Cruz Padua, B., Rossoni Junior, J.V., Brito Magalhaes, C.L. de, Seiberf, J.B., Araujo, C. M., Bianco de Souza, G.H., Chaves, M.M., Silva, M.E., Pedrosa, M.L., Costa, D.C., 2013. *Baccharis trimera* improves the antioxidant defense system and inhibits iNOS and NADPH oxidase expression in a rat model of inflammation. Curr. Pharm. Biotechnol. 14, 975–984. https://doi.org/10.2174/1389201014666131226151728.

Da Kim, B., Unenkhuu, B., Kim, G.J., Kim, S.-W., Kim, H.S., 2022. Cynarin attenuates LPS-induced endothelial inflammation via upregulation of the negative regulator MKP-3. Anim. Cell Syst. 26, 119–128. https://doi.org/10.1080/19768354.2022.2077438.

Da Mendes, L.C., Dantas, T.B.V., Severino, R.P., Da Silva, L.R.G., Souza, D.H.F. de, Cass, Q.B., Ramalho, S.D., Vieira, P.C., Souza, G.E. de, Guido, R.V.C., Urschel, M.-K., Kersten, C., Sousa, L.R.F. de, 2023. Using molecular networking and docking to explore arginase inhibitors among *Drimys brasiliensis* chemical constituents. Med. Chem. Res. 32, 2208–2218. https://doi.org/10.1007/s00044-023-03123-w.

Da Silva, C.F., Wihelms, R.Z., Queiroz Júnior, L.H.K., Dos Santos, N.C.F., Oliveira, A.E. de, Lopes, P.S., Costa, L.S., Severino, M.R., Sousa, L.R.F. de, Macedo, A.P.M.G., Severino, V.G.P., 2025. Chemical profiling and cosmeceutical potential of *Hymenaea stigonocarpa* fruit peel and seeds. Food Chem. 493, 145961. https://doi.org/10.1016/j.foodchem.2025.145961.

Della Sahid, E.N., Claudino, J.C., Oda, F.B., Carvalho, F.A., Santos, A.G.D., Graminha, M. A.S., Da Clementino, L.C., 2022. *Baccharis trimera* (Less.) DC leaf derivatives and eupatorin activities against Leishmania amazonensis. Nat. Prod. Res. 36, 1599–1603. https://doi.org/10.1080/14786419.2021.1887175.

Dührkop, K., Fleischauer, M., Ludwig, M., Aksenov, A.A., Melnik, A.V., Meusel, M., Dorrestein, P.C., Rousu, J., Böcker, S., 2019. Sirius 4: a rapid tool for turning tandem mass spectra into metabolite structure information. Nat. Methods 16, 299–302. https://doi.org/10.1038/s41592-019-0344-8.

Dührkop, K., Nothias, L.F., Fleischauer, M., Reher, R., Ludwig, M., Hoffmann, M.A., Petras, D., Gerwick, W.H., Rousu, J., Dorrestein, P.C., Böcker, S., 2021. Systematic classification of unknown metabolites using high-resolution fragmentation mass spectra. Nat. Biotechnol. 39, 462–471. https://doi.org/10.1038/s41587-020-0740-8.

Dührkop, K., Shen, H., Meusel, M., Rousu, J., Böcker, S., 2015. Searching molecular structure databases with tandem mass spectra using CSI:FingerID. Proc. Natl. Acad. Sci. U. S. A 112, 12580–12585. https://doi.org/10.1073/pnas.1509788112.

Dickel, M.L., Rates, S.M.K., Ritter, M.R., 2007. Plants popularly used for loosing weight purposes in Porto Alegre, South Brazil. J. Ethnopharmacol. 109, 60–71. https://doi.org/10.1016/j.jep.2006.07.003.

Duarte, M.C.T., Figueira, G.M., Sartoratto, A., Rehder, V.L.G., Delarmelina, C., 2005. Anti-candida activity of Brazilian medicinal plants. J. Ethnopharmacol. 97, 305–311. https://doi.org/10.1016/j.jep.2004.11.016.

Es-Safi, N.-E., Kerhoas, L., Ducrot, P.-H., 2005. Application of positive and negative electrospray ionization, collision-induced dissociation and tandem mass spectrometry to a study of the fragmentation of 6-hydroxyluteolin 7-O-glucoside and 7-O-glucosyl-(1→3)-glucoside. Rapid Commun. Mass Spectrom.: RCM (Rapid Commun. Mass Spectrom.) 19, 2734–2742. https://doi.org/10.1002/rcm.2122.

Filipova, M., Elhelu, O.K., Paoli, S.H. de, Fremuntova, Z., Mosko, T., Cmarko, D., Simak, J., Holada, K., 2018. An effective "three-in-one" screening assay for testing drug and nanoparticle toxicity in human endothelial cells. PLoS One 13, e0206557. https://doi.org/10.1371/journal.pone.0206557.

Fitoterapia Brasil, 2025. Baccharis trimera. https://fitoterapiabrasil.com.br/planta-medicinal/baccharis-trimera. (Accessed 20 November 2025).

Frusciante, L., Geminiani, M., Olmastroni, T., Mastroeni, P., Trezza, A., Salvini, L., Lamponi, S., Spiga, O., Santucci, A., 2024. Repurposing castanea sativa spiny burr By-Products extract as a potentially effective anti-inflammatory agent for novel future biotechnological applications. Life 14, 763. https://doi.org/10.3390/life14060763.

Ge, J., Liu, Z., Zhong, Z., Wang, L., Zhuo, X., Li, J., Jiang, X., Ye, X.Y., Xie, T., Bai, R., 2022. Natural terpenoids with anti-inflammatory activities: potential leads for anti-inflammatory drug discovery. Bioorg. Chem. 124, 105817. https://doi.org/10.1016/j.bioorg.2022.105817.

Goenka, S., 2025. Effects of sinensetin, Eupatilin, and Jaceosidin on human melanogenesis: a pilot study. Future Pharmacol. 5, 12. https://doi.org/10.3390/futurepharmacol5010012.

Gonçalves Neto, G., Da Costa, R., Zanini, C., Aguiar, A.C., Souza, J. de, Souza, G. de, Severino, R., Cass, Q., Cruz, F., Oliva, G., Guido, R., Sousa, L. de, 2020. Chemical prospection of *Qualea grandiflora* Mart. Fruit and stem extracts and their in vitro and in vivo antiplasmodial activity. J. Braz. Chem. Soc. https://doi.org/10.21577/0103-5053.20200034.

Guan, S., Sun, L., Wang, X., Huang, X., Luo, T., 2022. Isoschaftoside inhibits lipopolysaccharide-induced inflammation in microglia through regulation of HIF-1α-Mediated metabolic reprogramming. Evid. Based Complement. Alternat. Med.: eCAM 2022, 5227335. https://doi.org/10.1155/2022/5227335.

Hwang, J.-H., Lee, B.M., 2007. Inhibitory effects of plant extracts on tyrosinase, L-DOPA oxidation, and melanin synthesis. J. Toxicol. Environ. Health, Part A 70, 393–407. https://doi.org/10.1080/10937400600882871.

Ismaya, W.T., Rozeboom, H.J., Weijn, A., Mes, J.J., Fusetti, F., Wichers, H.J., Dijkstra, B. W., 2011. Crystal structure of Agaricus bisporus mushroom tyrosinase: identity of the tetramer subunits and interaction with tropolone. Biochemistry 50, 5477–5486. https://doi.org/10.1021/bi200395t.

Jakimiuk, K., Gesek, J., Atanasov, A.G., Tomczyk, M., 2021. Flavonoids as inhibitors of human neutrophil elastase. J. Enzym. Inhib. Med. Chem. 36, 1016–1028. https://doi.org/10.1080/14756366.2021.1927006.

Jan, K.C., Gavahian, M., 2024. Hydroxylated tetramethoxyflavone affects intestinal cell permeability and inhibits cytochrome P450 enzymes. Molecules 29, 322. https://doi.org/10.3390/molecules29020322.

Kang, J.Y., Xu, M.M., Sun, Y., Ding, Z.X., Wei, Y.Y., Zhang, D.W., Wang, Y.G., Shen, J.L., Wu, H.M., Fei, G.-H., 2022. Melatonin attenuates LPS-Induced pyroptosis in acute lung injury by inhibiting NLRP3-GSDMD pathway via activating Nrf2/HO-1 signaling axis. Int. Immunopharmacol. 109, 108782. https://doi.org/10.1016/j.intimp.2022.108782.

Kanlayavattanakul, M., Lourith, N., Chaikul, P., 2018. Biological activity and phytochemical profiles of dendrobium: a new source for specialty cosmetic materials. Ind. Crop. Prod. 120, 61–70. https://doi.org/10.1016/j.indcrop.2018.04.059.

Karaoğlan, E.S., Koca, M., 2020. Tyrosinase, cholinesterase inhibitory activity and molecular docking studies on apigenin and vitexin. Istanbul J. Pharm. 50, 236–244. https://doi.org/10.26650/IstanbulJPharm.2019.0076.

Kim, H.W., Wang, M., Leber, C.A., Nothias, L.F., Reher, R., Kang, K.B., van der Hooft, J.J. J., Dorrestein, P.C., Gerwick, W.H., Cottrell, G.W., 2021. NPClassifier: a deep neural network-based structural classification tool for natural products. J. Nat. Prod. 84, 2795–2807. https://doi.org/10.1021/acs.jnatprod.1c00399.

Kim, M.J., Han, J.M., Jin, Y.Y., Baek, N.I., Bang, M.H., Chung, H.G., Choi, M.S., Lee, K.T., Sok, D.E., Jeong, T.S., 2008. In vitro antioxidant and anti-inflammatory activities of Jaceosidin from *Artemisia princeps* Pampanini cv. Sajabal. Arch Pharm. Res. (Seoul) 31, 429–437. https://doi.org/10.1007/s12272-001-1175-8.

Kim, J.H., Kang, N.J., 2015. Potent whitening effects of rutin metabolites. Korean J. Food Preserv. 22, 607–612. https://doi.org/10.11002/kjfp.2015.22.4.607.

Kisiel, W., Barszcz, B., 1997. Minor sesquiterpene lactones from *Lactuca virosa*. Phytochemistry 46, 1241–1243. https://doi.org/10.1016/S0031-9422(97)80019-2.

Koch, W., Zagórska, J., Marzec, Z., Kukula-Koch, W., 2019. Applications of tea (*Camellia sinensis*) and its active constituents in cosmetics. Molecules 24, 4277. https://doi.org/10.3390/molecules24234277.

Koh, T.J., DiPietro, L.A., 2011. Inflammation and wound healing: the role of the macrophage. Expert Rev. Mol. Med. 13, e23. https://doi.org/10.1017/S1462399411001943.

Korkmaz, B., Horwitz, M.S., Jenne, D.E., Gauthier, F., 2010. Neutrophil elastase, proteinase 3, and cathepsin G as therapeutic targets in human diseases. Pharmacol. Rev. 62, 726–759. https://doi.org/10.1124/pr.110.002733.

Laavola, M., Nieminen, R., Yam, M.F., Sadikun, A., Asmawi, M.Z., Basir, R., Welling, J., Vapaatalo, H., Korhonen, R., Moilanen, E., 2012. Flavonoids eupatorin and sinensetin present in *Orthosiphon stamineus* leaves inhibit inflammatory gene expression and STAT1 activation. Planta Med. 78, 779–786. https://doi.org/10.1055/s-0031-1298458.

Leal, L.K.A.M., Canuto, K.M., Da Silva Costa, K.C., Nobre-Júnior, H.V., Vasconcelos, S.M., Silveira, E.R., Ferreira, M.V.P., Fontenele, J.B., Andrade, G.M., Barros Viana, G.S. de, 2009. Effects of amburoside A and isokaempferide, polyphenols from *Amburana cearensis*, on rodent inflammatory processes and myeloperoxidase activity in human neutrophils. Basic Clin. Pharmacol. Toxicol. 104, 198–205. https://doi.org/10.1111/j.1742-7843.2008.00329.x.

Lee, I.C., Bae, J.S., 2016. Anti-inflammatory effects of vicenin-2 and scolymoside on polyphosphate-mediated vascular inflammatory responses. Inflamm. Res. 65, 203–212. https://doi.org/10.1007/s00011-015-0906-x.

Li, L., Chen, Y., Feng, X., Yin, J., Li, S., Sun, Y., Zhang, L., 2019. Identification of metabolites of *eupatorin* in vivo and in vitro based on UHPLC-Q-TOF-MS/MS. Molecules 24, 2658. https://doi.org/10.3390/molecules24142658.

Li, W., Koike, K., Liu, L., Lin, L., Fu, X., Chen, Y., Nikaido, T., 2004. New lignan glucosides from the stems of *Tinospora sinensis*. Chem. Pharmaceut. Bull. 52, 638–640. https://doi.org/10.1248/cpb.52.638.

Lianza, M., Mandrone, M., Chiocchio, I., Tomasi, P., Marincich, L., Poli, F., 2020. Screening of ninety herbal products of commercial interest as potential ingredients for phytocosmetics. J. Enzym. Inhib. Med. Chem. 35, 1287–1291. https://doi.org/10.1080/14756366.2020.1774571.

Ludwig, M., Nothias, L.-F., Dührkop, K., Koester, I., Fleischauer, M., Hoffmann, M.A., Petras, D., Vargas, F., Morsy, M., Aluwihare, L., Dorrestein, P.C., Böcker, S., 2020. Database-independent molecular formula annotation using Gibbs sampling through ZODIAC. Nat. Mach. Intell. 2, 629–641. https://doi.org/10.1038/s42256-020-00234-6.

Martinez, M.J.A., Bessa, A.L., Benito, P.B., 2005. Biologically active substances from the genus *Baccharis* L. (Compositae). In: Atta-ur-Rahman (Ed.), Studies in Natural Products Chemistry: Bioactive Natural Products (Part K), 30. Elsevier, pp. 703–759. https://doi.org/10.1016/S1572-5995(05)80045-6.

Medeiros, V.G., Durán, F.J., Lang, K.L., 2021. Copalic acid: occurrence, chemistry, and biological activities. Revista Brasileira de Farmacognosia 31, 375–386. https://doi.org/10.1007/s43450-021-00173-2.

Midorikawa, K., Banskota, A., Tezuka, Y., Matsushige, K., Message, D., Huertas, A., Kadota, S., 2003. Buds of *Baccharis dracunculifolia*: potent source of biologically active caffeoylquinic acids and labdane-type diterpenes of Brazilian propolis. J. Ethnopharmacol. 84, 187–194. https://toyama.repo.nii.ac.jp/records/5250.

Ministério da Saúde, 2025. Plantas Medicinais de Interesse ao SUS – renisus. https://www.gov.br/saude/pt-br/composicao/sectics/plantas-medicinais-e-fitoterapicos/ppnpmf/renisus. (Accessed 20 November 2025).

Morais, L., Castanha, R.F., 2011. Composição química do óleo essencial de duas amostras de carqueja (*Baccharis* sp.) coletadas em Paty do Alferes - Rio de Janeiro. Rev. Bras. Plantas Med. 13, 628–632. https://doi.org/10.1590/S1516-05722011000500020.

Morita, N., Shimizu, M., Arisawa, M., 1973. Two new flavone glycosides from *Cirsium lineare*. Phytochemistry 12, 421–423. https://doi.org/10.1016/0031-9422(73)80032-9.

Nhiem, N.X., Hien, N.T.T., Tai, B.H., Le Anh, H.T., Hang, D.T.T., Quang, T.H., van Kiem, P., van Minh, C., Ko, W., Lee, S., Oh, H., Kim, S.H., Kim, Y.H., 2015. New ent-kauranes from the fruits of *Annona glabra* and their inhibitory nitric oxide production in LPS-stimulated RAW264.7 macrophages. Bioorg. Med. Chem. Lett 25, 254–258. https://doi.org/10.1016/j.bmcl.2014.11.059.

Nunes, T., Souza, H.S. de, 2013. Inflammasome in intestinal inflammation and cancer. Mediat. Inflamm. 2013, 654963. https://doi.org/10.1155/2013/654963.

Oliveira, R.N. de, Rehder, V.L.G., Santos Oliveira, A.S., Júnior, Í.M., Carvalho, J.E. de, Ruiz, A.L.T.G. de, Jeraldo, V.d.L.S., Linhares, A.X., Allegretti, S.M., 2012. *Schistosoma mansoni*: in vitro schistosomicidal activity of essential oil of Baccharis trimera (less) DC. Exp. Parasitol. 132, 135–143. https://doi.org/10.1016/j.exppara.2012.06.005.

Pieroni, A., Quave, C.L., Villanelli, M.L., Mangino, P., Sabbatini, G., Santini, L., Boccetti, T., Profili, M., Ciccioli, T., Rampa, L.G., Antonini, G., Girolamini, C., Cecchi, M., Tomasi, M., 2004. Ethnopharmacognostic survey on the natural ingredients used in folk cosmetics, cosmeceuticals and remedies for healing skin diseases in the inland Marches, Central-Eastern Italy. J. Ethnopharmacol. 91, 331–344. https://doi.org/10.1016/j.jep.2004.01.015.

Pillaiyar, T., Manickam, M., Namasivayam, V., 2017. Skin whitening agents: medicinal chemistry perspective of tyrosinase inhibitors. J. Enzym. Inhib. Med. Chem. 32, 403–425. https://doi.org/10.1080/14756366.2016.1256882.

Pranskuniene, Z., Grisiute, R., Pranskunas, A., Bernatoniene, J., 2022. Ethnopharmacology for skin diseases and cosmetics during the COVID-19 pandemic in Lithuania. Int. J. Environ. Res. Publ. Health 19, 4054. https://doi.org/10.3390/ijerph19074054.

Raju, K.S.R., Kadian, N., Taneja, I., Wahajuddin, M., 2015. Phytochemical analysis of isoflavonoids using liquid chromatography coupled with tandem mass spectrometry. Phytochemem. Rev. 14, 469–498. https://doi.org/10.1007/s11101-015-9400-x.

Ramos Campos, F., Bressan, J., Godoy Jasinski, V.C., Zuccolotto, T., Da Silva, L.E., Bonancio Cerqueira, L., 2016. *Baccharis* (Asteraceae): chemical constituents and biological activities. Chem. Biodivers. 13, 1–17. https://doi.org/10.1002/cbdv.201400363.

Rayamajhi, M., Zhang, Y., Miao, E.A., 2013. Detection of pyroptosis by measuring released lactate dehydrogenase activity. Methods Mol. Biol. 1040, 85–90. https://doi.org/10.1007/978-1-62703-523-1_7.

Razgonova, M.P., Bazhenova, B.A., Zabalueva, Y.Y., Burkhanova, A.G., Zakharenko, A. M., Kupriyanov, A.N., Sabitov, A.S., Ercisli, S., Golokhvast, K.S., 2022. Rosa *davurica Pall.*, Rosa *rugosa Thumb.*, and Rosa *acicularis Lindl.* Originating from far Eastern Russia: screening of 146 chemical constituents in three species of the genus Rosa. Appl. Sci. 12, 9401. https://doi.org/10.3390/app12199401.

Rodrigues, C.R.F., Dias, J.H., Mello, R.N. de, Richter, M.F., Picada, J.N., Ferraz, A.B.F., 2009. Genotoxic and antigenotoxic properties of *Baccharis trimera* in mice. J. Ethnopharmacol. 125, 97–101. https://doi.org/10.1016/j.jep.2009.06.006.

Sabir, S.M., Athayde, M.L., Boligon, A.A., Rocha, J., 2017. Antioxidant activities and phenolic profile of *Baccharis trimera*, a commonly used medicinal plant from Brazil. South Afr. J. Bot. 113, 318–323. https://doi.org/10.1016/j.sajb.2017.09.010.

Salem, M.A., El-Shiekh, R.A., Hashem, R.A., Hassan, M., 2021. In vivo antibacterial activity of star anise (Illicium verum Hook.) extract using murine MRSA skin infection model in relation to its metabolite profile. Infect. Drug Resist. 14, 33–48. https://doi.org/10.2147/IDR.S285940.

Sareedenchai, V., Zidorn, C., 2010. Flavonoids as chemosystematic markers in the tribe Cichorieae of the Asteraceae. Biochem. Systemat. Ecol. 38, 935–957. https://doi.org/10.1016/j.bse.2009.09.006.

Satheeshkumar, N., Shantikumar, S., Komali, M., 2014. Identification and quantification of aldose reductase inhibitory flavonoids in herbal formulation and extract of *Gymnema sylvestre* using HPLC-PDA and LC-MS/MS. Chromatogr. Res. Int. 1–8. https://doi.org/10.1155/2014/518175, 2014.

Schmid, R., Heuckeroth, S., Korf, A., Smirnov, A., Myers, O., Dyrlund, T.S., Bushuiev, R., Murray, K.J., Hoffmann, N., Lu, M., Sarvepalli, A., Zhang, Z., Fleischauer, M., Dührkop, K., Wesner, M., Hoogstra, S.J., Rudt, E., Mokshyna, O., Brungs, C., Ponomarov, K., Mutabdžija, L., Damiani, T., Pudney, C.J., Earll, M., Helmer, P.O., Fallon, T.R., Schulze, T., Rivas-Ubach, A., Bilbao, A., Richter, H., Nothias, L.-F., Wang, M., Orešič, M., Weng, J.-K., Böcker, S., Jeibmann, A., Hayen, H., Karst, U., Dorrestein, P.C., Petras, D., Du, X., Pluskal, T., 2023. Integrative analysis of multimodal mass spectrometry data in MZmine 3. Nat. Biotechnol. 41, 447–449. https://doi.org/10.1038/s41587-023-01690-2.

Serhan, C.N., 2014. Pro-resolving lipid mediators are leads for resolution physiology. Nature 510, 92–101. https://doi.org/10.1038/nature13479.

Shawl, A.S., Mengi, N., Kaul, M.K., Vishwapaul, 1988. Flavonoids of *Iris spuria*. Phytochemistry 27, 1559–1560. https://doi.org/10.1016/0031-9422(88)80245-0.

Shen, H., Dührkop, K., Böcker, S., Rousu, J., 2014. Metabolite identification through multiple kernel learning on fragmentation trees. Bioinformatics 30, i157–i164. https://doi.org/10.1093/bioinformatics/btu275.

Shin, M.S., Park, J.Y., Lee, J., Yoo, H.H., Hahm, D.H., Lee, S.C., Lee, S., Hwang, G.S., Jung, K., Kang, K.S., 2017. Anti-inflammatory effects and corresponding mechanisms of cirsimaritin extracted from *Cirsium japonicum* var. *maackii* Maxim. Bioorg. Med. Chem. Lett 27, 3076–3080. https://doi.org/10.1016/j.bmcl.2017.05.051.

Silva, A.N.C., Pereira, D.M.S., Andrade, E.C., Silveira, P.P.d.S., Silva, M.d.R.A.N., Da Rodrigues, K.C., Carneiro, M.F., Araújo, E.C.S. de, Da Silva, E.B., Da Silva, A.F.J., 2024. Fitocosméticos: benefícios de cosméticos de origem natural na estética. RevistaFT 28, 24–25. https://doi.org/10.69849/revistaft/ni10202410312124.

Silva, M.L., Oliveira, C.S., Dos Santos, W.J.O., Oliveira, V.X., Antar, G.M., Lago, J.H.G., Cerchiaro, G., 2022. Selective cytotoxicity of ent-kaurene diterpenoids isolated from *Baccharis lateralis* and *Baccharis retusa* (Asteraceae). Arch. Pharmazie 355, e2200083. https://doi.org/10.1002/ardp.202200083.

Silveira Rabelo, A.C., Caldeira Costa, D., 2018. A review of biological and pharmacological activities of *Baccharis trimera*. Chem. Biol. Interact. 296, 65–75. https://doi.org/10.1016/j.cbi.2018.09.002.

Song, S.-Y., Lee, S.-H., Bae, M.-S., Park, D.-H., Cho, S.-S., 2023. Strong inhibition of xanthine oxidase and elastase of Baccharis trimera (Less.) DC stem extract and analysis of biologically active constituents. Front. Pharmacol. 14, 1160330. https://doi.org/10.3389/fphar.2023.1160330.

Song, W.Y., Kim, N.J., Kim, S.Y., Lee, H.S., 2009. Liquid chromatography-tandem mass spectrometry for the determination of jaceosidin in rat plasma. J. Pharmaceut. Biomed. Anal. 49, 381–386. https://doi.org/10.1016/j.jpba.2008.10.021.

Souza, F. de, Brito, L., Silva, M., Sugimoto, M., Pinto, A.C., Almeida, P. de, Souza, R., Costa, R., Guilhon-Simplicio, F., Wanderley, A., Oliveira, K. de, Sousa, L., Da Veiga-Junior, V., Lima, E., 2020. Synthesis, Characterization and in vitro, in vivo and in silico anti-inflammatory studies of the novel hybrid based on ibuprofen and 3-hydroxy-copalic acid isolated from copaiba oil (*Copaifera multijuga*). J. Braz. Chem. Soc. 31, 1335–1344. https://doi.org/10.21577/0103-5053.20190266.

Souza Vargas, F. de, D O de Almeida, P., Aranha, E.S.P., A Boleti, A.P. de, Newton, P., Vasconcellos, M.C. de, Junior, V.F.V., Lima, E.S., 2015. Biological activities and cytotoxicity of diterpenes from Copaifera spp. oleoresins. Molecules 20, 6194–6210. https://doi.org/10.3390/molecules20046194.

Unver, N., Freyschmidt-Paul, P., Hörster, S., Wenck, H., Stäb, F., Blatt, T., Elsässer, H.-P., 2006. Alterations in the epidermal-dermal melanin axis and factor XIIIa melanophages in senile lentigo and ageing skin. Br. J. Dermatol. 155, 119–128. https://doi.org/10.1111/j.1365-2133.2006.07210.x.

Verdi, L.G., Brighente, I.M.C., Pizzolatti, M.G., 2005. Gênero Baccharis (Asteraceae): aspectos químicos, econômicos e biológicos. Quim. Nova 28, 85–94. https://doi.org/10.1590/S0100-40422005000100017.

Videira, I.F.d.S., Moura, D.F.L., Magina, S., 2013. Mechanisms regulating melanogenesis. An. Bras. Dermatol. 88, 76–83. https://doi.org/10.1590/s0365-05962013000100009.

Wang, M., Carver, J.J., Phelan, V.V., 2016. Sharing and community curation of mass spectrometry data with Global Natural Products Social Molecular Networking. Nat. Biotechnol. 34 (8), 828–837. https://doi.org/10.1038/nbt.3597.

Wu, C., Chen, F., Wang, X., Wu, Y., Dong, M., He, G., Galyean, R.D., He, L., Huang, G., 2007. Identification of antioxidant phenolic compounds in feverfew (Tanacetum parthenium) by HPLC-ESI-MS/MS and NMR. Phytochem. Anal.: PCA (Phytochem. Anal.) 18, 401–410. https://doi.org/10.1002/pca.995.

Wu, C.Y., Khan, M., Ding, H.Y., Wang, T.Y., Li, Y.X., Liu, C.W., Wu, J.Y., Chang, T.S., 2025. Biotransformation: a novel approach for the production of 6-hydroxyluteolin 7- *O*-methylglucuronide compound with antioxidant and anti-inflammatory potential. Nat. Prod. Res. 1–8. https://doi.org/10.1080/14786419.2025.2536633.

Ximenes, T.V.N., Carvalho, R., Bonfá, I.S., Santos, V.S., Candeloro, L., Alves, F.M., Silva, D.B., Carollo, C.A., Gielow, K.d.C.F., Silva-Filho, S.E., Toffoli-Kadri, M.C., 2022. *Baccharis trimera* Infusion reduces macrophages activation and high-fat diet-induced metabolic disorders in mice. Pharmaceuticals 15, 1258. https://doi.org/10.3390/ph15101258.

Xu, Z.P., Liu, Y., Wang, S.Y., Li, Z.W., Lu, D.X., Jiang, P., Pan, J., Guan, W., Kuang, H.X., Yang, B.Y., 2022. Phenolic compounds of *Solanum xanthocarpum* play an important role in anti-inflammatory effects. Arab. J. Chem. 15, 103877. https://doi.org/10.1016/j.arabjc.2022.103877.

Xue, P., Wang, Y., Zeng, F., Xiu, R., Chen, J., Guo, J., Yuan, P., Liu, L., Xiao, J., Lu, H., Wu, D., Pan, H., Lu, M., Zhu, F., Shi, F., Duan, Q., 2017. Paeonol suppresses solar ultraviolet-induced skin inflammation by targeting T-LAK cell-originated protein kinase. Oncotarget 8, 27093–27104. https://doi.org/10.18632/oncotarget.15636.

Yang, C.-C., Hsiao, L.-D., Shih, Y.-F., Lin, H.-H., Yang, C.-M., 2022. 5,8-Dihydroxy-4 ‘, 7-dimethoxyflavone attenuates TNF-α-induced expression of vascular cell adhesion molecule-1 through EGFR/PKCα/PI3K/Akt/Sp1-dependent induction of heme oxygenase-1 in human cardiac fibroblasts. Oxid. Med. Cell. Longev. 2022, 1372958. https://doi.org/10.1155/2022/1372958.

Zhang, X., Liao, M., Cheng, X., Liang, C., Diao, X., Zhang, L., 2018. Ultrahigh-performance liquid chromatography coupled with triple quadrupole and time-of-flight mass spectrometry for the screening and identification of the main flavonoids and their metabolites in rats after oral administration of *Cirsium japonicum* DC. extract. Rapid Commun. Mass Spectrom.: RCM (Rapid Commun. Mass Spectrom.) 32, 1451–1461. https://doi.org/10.1002/rcm.8161.

Zhang, X.W., Bian, G.L., Kang, P.Y., Cheng, X.J., Yan, K., Liu, Y.L., Gao, Y.X., Li, D.Q., 2021. Recent advance in the discovery of tyrosinase inhibitors from natural sources via separation methods. J. Enzym. Inhib. Med. Chem. 36, 2104–2117. https://doi.org/10.1080/14756366.2021.1983559.

Zolghadri, S., Bahrami, A., Hassan Khan, M.T., Munoz-Munoz, J., Garcia-Molina, F., Garcia-Canovas, F., Saboury, A.A., 2019. A comprehensive review on tyrosinase inhibitors. J. Enzym. Inhib. Med. Chem. 34, 279–309. https://doi.org/10.1080/14756366.2018.1545767.